Faddeev calculations for low-energy *p-d* scattering

G. H. Berthold
Department of Physics and Astronomy, University of New Mexico, Albuquerque, New Mexico 87131

A. Stadler
Institut für Theoretische Physik, Universität Hannover, 3000 Hannover 1, Federal Republic of Germany

H. Zankel
Institut für Theoretische Physik, Karl-Franzens-Universität Graz, 8010 Graz, Austria
(Received 10 October 1989)

The Coulomb-modified Faddeev equations were solved in momentum space for different separable potential models at $E_{\rm lab}^{p}=2.5$ and 3.0 MeV. The best agreement with available experimental data of zero- and first-order spin polarization observables was achieved by employing a separable approximation of the Paris potential in the calculation. These results, together with predictions of second-order *p-d* polarizations, demonstrate the necessity of a correct treatment of three-body Coulomb corrections. Moreover, no indication of model sensitivity is found in our results. Three-nucleon phase shift parameters are given and the validity of a simple approximate two-body description of the three-body Coulomb corrections is discussed.

I. INTRODUCTION

Including the effects of the Coulomb interaction in calculations for the three-nucleon systems has been a long standing goal. In this paper we present the results of an elaborate calculation for proton-deuteron (*p-d*) scattering at proton laboratory energies of 2.5 and 3.0 MeV.

Aside from direct interest in the *p-d* system for its own sake, there is a more fundamental reason for the need to include Coulomb effects accurately. Despite the fact that an exact theory has been in existence for nearly 30 years, the nuclear three-body system has not been the expected source of information on aspects of the *N-N* interaction typically not accessible through *N-N* scattering. Though very elaborate calculations have been performed with different *N-N* interaction models of various levels of sophistication, knowledge about the spin dependence and the off-shell component of the *N-N* interaction has not been significantly improved. Both theory and experiment have to be blamed for this uncomfortable situation, but nature has indeed made progress quite expensive through the presence of the Coulomb force. What is advantageous for the three-body scattering experiments, namely the electric charge of the protons, turns out to be a major obstacle for the theoretical description of proton-deuteron (*p-d*) scattering. In fact, the vast majority of the three-nucleon experiments are *p-d* data whereas the calculations were performed without a proper treatment of the Coulomb force; i.e., the calculations were only suited for electrically neutral scattering as given by neutron-deuteron (*n-d*) scattering. Since all of the enlightening *p-d* polarization data have always been analyzed by *n-d* calculations, which employed rude approximations of the three-body Coulomb effect at best, no conclusive interpretation of the measurements was possible. Therefore, only the already difficult and sparse *n-d* measurements of the differential cross sections and neutron analyzing powers have provided a basis for studying *N-N* interaction models through *n-d* scattering equations.

In order to take advantage of the more abundant *p-d* data as a test for *N-N* potential models it is mandatory to properly incorporate the Coulomb force in the three-body equations. Because of the long-range nature of the Coulomb potential this aspect of the theory is by no means trivial and progress has been slow accordingly. An important first step towards establishing solvable exact *p-d* equations was achieved more than 10 years ago within the quasiparticle concept applied to Coulomb-modified three-body scattering.[1,2] Due to the complexity of the calculation only *N-N S* states have been employed, thus restricting the results to *p-d* differential cross sections which in turn do not reflect the spin dependence of the *N-N* interaction.

A few years later *p-d* scattering equations using again only *N-N S* states were solved in configuration space.[3,4] Another configuration space calculation performed at the elastic threshold energy by the Los Alamos–Iowa group[5–7] followed, stirring up a discussion on the validity of the configuration space results. Meanwhile, a momentum space calculation[8] and recent configuration space results for energies below the inelastic threshold[9,10] have independently cast doubt on the results of Kvitsinskii.[3]

The common feature of all *p-d* calculations yet available is their failure to describe spin polarization observables other than a few second-order ones that are dominated by *N-N S* states.[11] To benefit from the existing accurate *p-d* polarization data at various energies, namely below the breakup threshold, it is necessary to perform *p-d* calculations that take into account higher *N-N* partial waves and incorporate the Coulomb force correctly. Only then will it be sensible to discriminate among

different N-N force models on the basis of p-d scattering data and to consider three-body forces a possible source for discrepancies between theory and experiment.

In the past few years a project at the University of Graz was devoted to the Coulomb corrections in the three-nucleon system. The present work is a continuation of previously published work of this group,[8,11,12] and it represents the final result of the whole project. Here, we consider higher partial waves in the N-N potentials and calculate by means of the quasiparticle method for the first time p-d polarization observables that correctly contain three-body Coulomb corrections. In the next section the three-nucleon equations are discussed and in Sec. III the rank-one separable N-N potentials used in the calculation will be addressed. Section IV contains p-d and n-d observables at two energies below the breakup threshold. They are calculated with N-N potentials mainly different in their off-shell behavior. Furthermore, a phase shift representation of the three-nucleon scattering matrix is given (Sec. V) and Sec. VI contains a comparison of correct and approximate treatments of the Coulomb corrections in p-d scattering. In Sec. VII the results are summarized and, finally, the Appendix provides some details about parts of the three-body equations.

II. THREE-BODY EQUATIONS

In this paper we make use of the quasiparticle method first used by Alt and co-workers[1,2] to incorporate the Coulomb interaction in the three-nucleon momentum space Faddeev equations. These Coulomb-modified p-d Faddeev equations could be solved numerically by screening the Coulomb interaction and subsequently renormalizing the screened Coulomb modified on-shell scattering matrix. In our calculations we followed this same procedure expanding the equations of Refs. 1 and 2 to accommodate N-N states other than S states. This, of course, entailed a significant increase of coding work and computer time. Furthermore, we made use of a numerical procedure, described in Ref. 8, to handle the quasisingular behavior of the kernel of the integral equation that arises from the screened Coulomb interaction.

As usual within the quasiparticle method the two-particle strong interaction is represented by a separable potential. For the ppn three-particle system there is also a nonseparable term, namely the Coulomb interaction in only one subsystem, the pp system. Assuming an exponential screening of the Coulomb potential the potentials in the subsystem read

$$v_\alpha = |g_\alpha\rangle \lambda_\alpha \langle g_\alpha| + \delta_{\alpha 3} v_C \ , \qquad v_C(r) = \frac{e^2}{r} e^{-r/R} \ , \tag{1}$$

where λ is the strength parameter and g denotes the form factor of the separable potential, the analytical form of which is given in the next section. Here, the index α is the usual channel index, where α denotes the noninteracting particle. R, which denotes the screening radius, may be omitted further on. However, all quantities related to the Coulomb potential also depend on R. The subsystem t matrix, which is the input information for the Faddeev equations that disregard three-nucleon forces, is

$$t_\alpha(z) = |\tilde{g}_\alpha\rangle \tau_\alpha(z) \langle \tilde{g}_\alpha| + \delta_{\alpha 3} t_C(z) \ , \tag{2}$$

where t_C is the screened Coulomb t matrix. The form factors $|\tilde{g}_\alpha\rangle$ are defined by

$$|\tilde{g}_\alpha\rangle = [1 + \delta_{\alpha 3} g_0(z) t_C(z)] |g_\alpha\rangle \ , \tag{3}$$

$$\tau_\alpha(z) = [\lambda_\alpha^{-1} - \langle g_\alpha | g_0(z) + \delta_{\alpha 3} g_0(z) t_C(z) g_0(z) | g_\alpha \rangle]^{-1} \ , \tag{4}$$

when $g_0(z)$ is the free two-body propagator at the two-particle energy z. Inserting expressions (1)–(3) into the three-particle Faddeev equations leads to the well-known effective two-particle equations[1,2] for the three-body transition operator $\mathcal{T}_{\beta\alpha}$

$$\mathcal{T}_{\beta\alpha} = \mathcal{V}_{\beta\alpha} + \sum_\gamma \mathcal{V}_{\beta\gamma} \mathcal{G}_{0;\gamma} \mathcal{T}_{\gamma\alpha} \ . \tag{5}$$

Here $\mathcal{G}_0$ is given in momentum space representation by

$$\langle \mathbf{q}'_\gamma | \mathcal{G}_{0;\gamma}(E) | \mathbf{q}_\gamma \rangle = \delta(\mathbf{q}'_\gamma - \mathbf{q}_\gamma) \tau_\gamma(E - \tfrac{3}{4} q_\gamma^2) \tag{6}$$

and $\mathcal{V}_{\beta\alpha}$ denotes the effective potential (cf. the Appendix). Equation (4) now reads in momentum space representation

$$\langle \mathbf{q}_\beta | \mathcal{T}_{\beta\alpha}(E) | \mathbf{q}_\alpha \rangle = \langle \mathbf{q}_\beta | \mathcal{V}_{\beta\alpha}(E) | \mathbf{q}_\alpha \rangle + \sum_\gamma \int d^3 q_\gamma \langle \mathbf{q}_\beta | \mathcal{V}_{\beta\gamma}(E) | \mathbf{q}_\gamma \rangle \tau_\gamma(E - \tfrac{3}{4} q_\gamma^2) \langle \mathbf{q}_\gamma | \mathcal{T}_{\gamma\alpha}(E) | \mathbf{q}_\alpha \rangle \ . \tag{7}$$

To derive one-dimensional integral equations we use a partial wave decomposition. In particular, we choose the channel spin coupling scheme to derive the basis states

$$|q_\alpha, N_\alpha\rangle \equiv |q_\alpha (\{[(\sigma_\beta \sigma_\gamma) s_\alpha l_\alpha] j_\alpha \sigma_\alpha\} S_\alpha L_\alpha) J J_z, [(\iota_\beta \iota_\gamma) i_\alpha \iota_\alpha] I_\alpha I_z\rangle \ . \tag{8}$$

The conserved quantum numbers are the total angular momentum J, the parity π and the z component of the total isospin I_z. The other quantum numbers are the particle spin σ, the total spin of the two-particle system s, the relative angular momentum l of these, the total angular momentum of the subsystem j, the channel spin S, the angular momentum L of the spectator relative to the subsystem, the isospin of one particle ι, the total isospin of the subsystem i, and the to-

tal isospin I_α. Thus the partial wave decomposed Coulomb-modified Faddeev equations, which are now a set of coupled one-dimensional integral equations, read

$$\mathcal{T}^{J\pi I_z}_{N_\beta N_\alpha}(q_\beta,q_\alpha;E)=\mathcal{V}^{J\pi I_z}_{N_\beta N_\alpha}(q_\beta,q_\alpha;E)+4\pi\sum_{\gamma\gamma'}\int_0^\infty dq_\gamma q_\gamma^2\,\mathcal{V}^{J\pi I_z}_{N_\beta N_\gamma}(q_\beta,q_\gamma;E)\mathcal{G}^{J\pi I_z}_{0;N_\gamma N_{\gamma'}}(E)\mathcal{T}^{J\pi I_z}_{N_{\gamma'}N_\alpha}(q_\gamma,q_\alpha;E)\ . \tag{9}$$

Note that, due to the Coulomb interaction, the effective propagator is no longer diagonal with respect to the isospin. The explicit form of $\mathcal{V}_{\beta\alpha}$ and $\mathcal{G}_{0;\gamma}$ can be found in the Appendix and a detailed derivation is given in Ref. 13. In those formulas the two-body subsystem Coulomb t matrix is consistently replaced by the Coulomb potential. Such an approximation significantly reduces computing requirements, and we expect the influence of the higher-order contributions to remain within the limits of our numerical accuracy.[14]

Since we always take a finite number of N-N states in practice, the actual number of coupled equations depends on the choice of the separable interaction model. Assuming only rank-one separable interaction in the N-N states (see the next section) we obtain the following maximal number $N_{\max}$ of coupled three-particle channels for a given set of conserved quantum numbers:

$$J=\tfrac{1}{2},\quad \pi=\pm,\quad I_z=\pm\tfrac{1}{2},\quad N_{\max}=10\ ,$$

$$J\geq\tfrac{3}{2},\quad \pi=\pm,\quad I_z=\pm\tfrac{1}{2},\quad N_{\max}=16\ .$$

Because we use charge-independent N-N interaction we assume that the $I=\frac{3}{2}$ states have a negligible contribution[12] and we consequently disregard them.

III. N-N INTERACTIONS

In order to keep the computing time for the solution of the p-d equations at an acceptable level, we had to restrict our choice of N-N potentials to rank-one separable potentials with form factors of a specific analytical form. The quality of the representation of the N-N data suffers throughout the first requirement of rank-one separable interactions, but, except for the D wave and the mixing parameter in the $^3S_1$-$^3D_1$ state, the N-N phase shifts are quite realistic up to about 100 MeV. Since we are calculating p-d scattering at low energies, the smaller subsystem N-N scattering energies should be predominant and the shortcomings of higher-energy N-N phase shifts not too crucial. The second requirement, originating from the intention to integrate analytically as much as possible in the effective potential of the Coulomb-modified Faddeev equations, does not seriously affect the quality of the N-N potentials. Although our spin-isospin representation of the three-nucleon equations would allow us to use charged-dependent N-N potentials (e.g., in the $^1S_0$ state) we have, for reason of comparison with existing n-d calculations, employed a charge-independent parametrization. We have considered for our calculation the $^1S_0$, $^3S_1$-$^3D_1$, $^1P_1$, $^3P_0$, $^3P_1$, and $^3P_2$ N-N states. The small D waves $^1D_2$ and $^3D_2$ as well as the $^3F_2$ coupled to $^3P_2$ were neglected because they do not contribute significantly to the three-nucleon scattering observables at energies such as $E^N_{\rm lab}=2.5$ MeV.[15,16]

Two sets of potentials are used here. The first set is a separable approximation of the Paris potential[17] where the form factors of this so-called PEST16 potential have the following form:

$$g_{n_\alpha}(p)=\sum_{k=1}^{6}\frac{c_{k,n_\alpha}}{p^2+\beta^2_{k,n_\alpha}}\quad\text{for } {}^1S_0,{}^3S_1\ ,$$

$$g_{n_\alpha}(p)=\sum_{k=1}^{6}\frac{c_{k,n_\alpha}p^2}{(p^2+\beta^2_{k,n_\alpha})^2}\quad\text{for } {}^3D_1\ , \tag{10}$$

$$g_{n_\alpha}(p)=\sum_{k=1}^{6}\frac{c_{k,n_\alpha}p}{(p^2+\beta^2_{k,n_\alpha})^2}\quad\text{for } {}^1P_1,{}^3P_0,{}^3P_1,{}^3P_2\ .$$

The potential parameters for the $^1S_0$ state, given in Ref. 18, for the coupled $^3S_1$-$^3D_1$ state, presented in Ref. 19, and for the P states[20] are listed in Table I. To study the model dependence of the three-nucleon Coulomb corrections, we have made use of a second set of potentials that guarantees rather similar N-N phase shifts (though not phase equivalent) but quite different half-off-shell behavior. The parameters of these one-term Yamaguchi-type potentials Y are also taken from the literature, namely for the $^1S_0$ and $^3S_1$-$^3D_1$ state from Ref. 19 whereby the tensor potential with 5.5% D-state probability, $Y5.5\%$, was chosen. The models for the $^1P_1$, $^3P_1$, $^3P_2$ states come from Ref. 21 and for the $^3P_0$ state from Ref. 15. A comparison of the phase shifts and the half-shell functions for both sets of potentials is contained in Table II and Fig. 1, together with the original results of the Paris potential.[22] It should be noted that for a rank-one separable potential only two independent half-off-shell functions can be obtained in the coupled channel and that consequently no comparison of the original Paris potential is given for the S-to-D-state transition

The PEST16 potential obviously should be considered vis-à-vis the p-d measurements provided that the Paris potential describes the N-N interaction in a realistic way. The $^3S_1$-$^3D_1$ mixing parameter and the $^3D_1$ phase shift produced by the PEST16 potential are certainly not realistic. On the other hand, the $^3S_1$ deuteron wave function or the static properties of the deuteron, which should show the biggest influence of the coupled channel on the low-energy three-nucleon observables, are exactly reproduced. Consequently, we expect the PEST16 potential to provide the more realistic description of low-energy p-d scattering.

For the purpose of studying the model dependence of the three-nucleon Coulomb corrections, the differences in the half-shell functions between the PEST16 potential and the Yamaguchi-like potentials seem to be significant enough, although the low-energy phase shifts of the two potential sets are quite similar. However, we do not em-

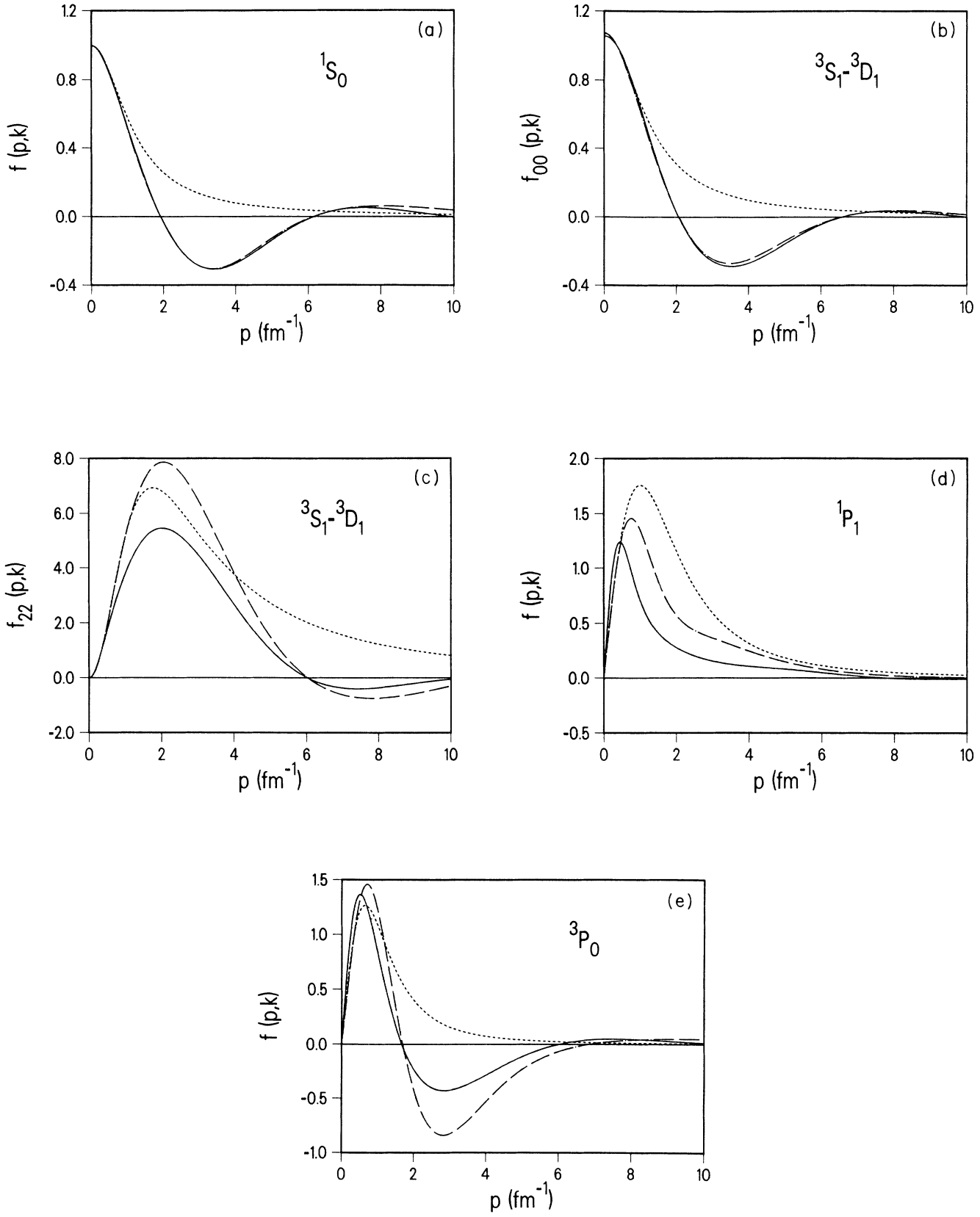

FIG. 1. Kowalski-Noyes half-off-shell functions (Refs. 42 and 43) for the Paris potential (solid line), the Y potentials (dashed line), and the PEST16 potential (dotted line). The functions were calculated at an on-shell momentum k corresponding to a nucleon energy of 10 MeV.

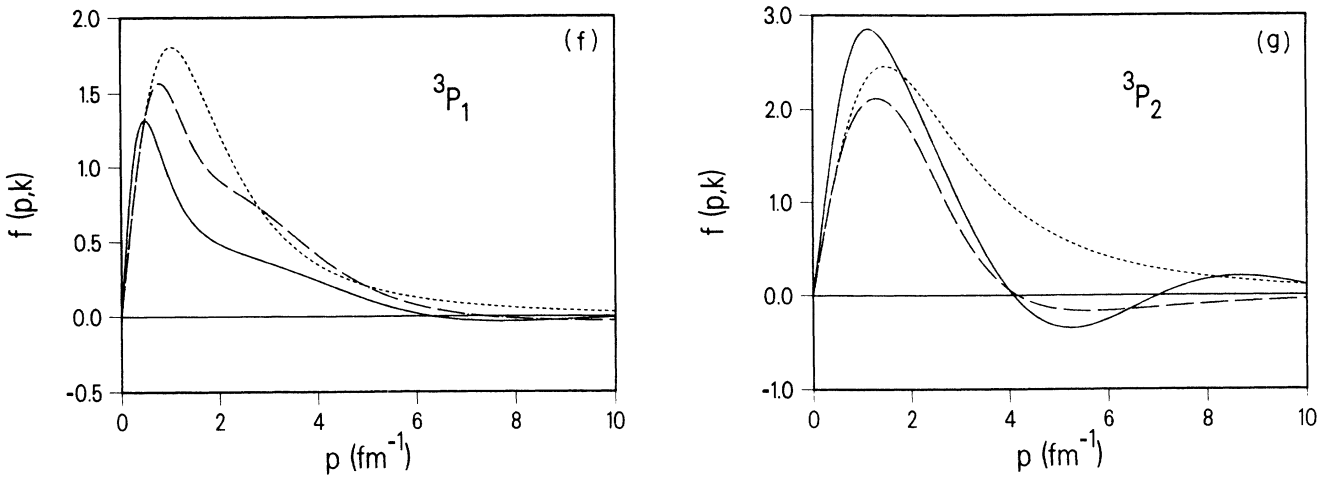

FIG. 1. (*Continued*).

TABLE I. Parameters of the PEST16 potential.

N-N state	λ (fm^{-2l-3})	k	β_k (fm^{-1})	c_k
$^1S_0$	$-2.446\,250\,0\times10^{-4}$	1	1.800 000	−337.1159
		2	2.924 109	9 469.785
		3	3.883 805	−81 980.88
		4	4.750 228	247 537.9
		5	5.553 305	−298 661.1
		6	6.309 259	124 526.1
$^3S_1$	$-1.191\,885\,3\times10^{-3}$	1	1.400 000	−9.791 345
		2	2.800 000	98.379 02
		3	4.200 000	−3 414.619
		4	5.600 000	16 678.69
		5	7.000 000	−26 922.61
		6	8.400 000	13 960.91
$^3D_1$	$-1.191\,885\,3\times10^{-3}$	1	1.400 000	6.664 677
		2	2.800 000	61.561 27
		3	4.200 000	81.457 14
		4	5.600 000	288.875 5
		5	7.000 000	−2 294.157
		6	8.400 000	2 148.119
$^1P_1$	$3.523\,076\,0\times10^{-4}$	1	0.700 000	−0.503 235
		2	1.352 311	42.444 41
		3	1.987 757	504.457 5
		4	2.612 492	−3 232.453
		5	3.229 383	6 300.488
		6	3.840 093	−3 721.678
$^3P_0$	$-2.244\,940\,7\times10^{-4}$	1	0.700 000	2.150 399
		2	1.306 246	−119.087 2
		3	1.881 513	1 128.572
		4	2.437 542	−8 094.117
		5	2.979 690	18 710.40
		6	3.511 027	−12 309.56
$^3P_1$	$4.648\,843\,9\times10^{-4}$	1	0.800 000	−2.248 705
		2	1.492 853	151.068 7
		3	2.150 300	−466.716 3
		4	2.785 762	−816.005 8
		5	3.405 360	4 831.970
		6	4.012 602	−4 029.700
$^3P_2$	$-4.301\,318\,3\times10^{-4}$	1	0.760 000	0.335 967
		2	1.520 000	−50.769 75
		3	2.280 000	782.662 4
		4	3.040 000	−5 042.711
		5	3.800 000	9 216.529
		6	4.560 000	−4 943.591

TABLE II. N-N phase shifts.

N-N state	Potential model	E_{lab} 5 MeV	10 MeV	20 MeV	50 MeV
$^1S_0$	Paris	59.953	56.91	50.97	38.74
	PEST16	59.83	56.13	48.90	33.75
	Y type	61.80	58.03	51.25	38.26
$^3S_1$	Paris	118.04	102.42	85.97	62.28
	PEST16	117.75	102.02	85.37	61.34
	$Y5.5\%$	118.53	103.31	87.65	66.60
$\epsilon(^3S_1$-$^3D_1)$	Paris	0.64	0.97	1.60	1.89
	PEST16	1.46	3.19	6.41	13.73
	$Y5.5\%$	1.51	3.34	6.79	14.88
$^3D_1$	Paris	−0.04	−0.34	−1.02	−6.77
	PEST16	−0.02	−0.38	0.06	1.87
	$Y5.5\%$	−0.02	−0.46	0.03	1.75
$^1P_1$	Paris	−1.63	−3.37	−6.05	−10.95
	PEST16	−0.88	−2.21	−5.00	−10.94
	Y type	−0.66	−1.69	−4.03	−10.51
$^3P_0$	Paris	1.93	4.26	7.92	11.82
	PEST16	1.06	2.88	6.84	11.94
	Y type	1.63	3.92	7.84	11.79
$^3P_1$	Paris	−1.08	−2.31	−4.39	−8.41
	PEST16	−0.58	−1.54	−3.69	−8.65
	Y type	−0.61	−1.58	−3.80	−10.08
$^3P_2$	Paris	0.26	0.74	1.96	5.73
	PEST16	0.28	0.78	2.03	5.98
	Y type	0.24	0.67	1.79	5.87

ploy on-shell equivalent potentials and our considerations of the model dependence are consequently rather qualitative.

IV. NUMERICAL RESULTS

The three-body equations described in Sec. II are solved numerically for different values of the screening radius of the Coulomb interaction. In practice we employ the numerical procedure already described in Refs. 8 and 19. Away from the quasisingular region of the effective potential for three-body on-shell momentum we have taken 12 mesh points for the momentum integration and 24 grid points for the angular integration. The on-shell Coulomb-modified screened hadronic three-nucleon T matrix $\mathcal{T}_{sC}^{JR}$ is found by subtracting from the total screened p-d T matrix the screened c.m. Coulomb p-d T matrix $\mathcal{T}_C^R$. Multiplying by a well-known phase factor[1,2] yields in the limit the unscreened Coulomb-modified quantity

$$\mathcal{T}^{J\pi I_z}_{sC,N_\beta N_\alpha}(q_\beta,q_\alpha;E) = \lim_{R\to\infty} Z^{-1/2}_{R,\beta}(q_\beta)\mathcal{T}^{J\pi I_z;R}_{sC,N_\beta N_\alpha}(q_\beta,q_\alpha;E)Z^{-1/2}_{R,\alpha}(q_\alpha) . \quad (11)$$

The phase factor $Z_{R,\alpha}$ can be easily calculated from the screened Coulomb phase shifts obtained from the equation for pure three-body Coulomb scattering, or from the variable phase method.[23] The screening limit is obtained numerically by calculating $\mathcal{T}_{sC}^R$ for a series of increasing values of screening radii and by multiplying with the renormalization factor. Numerical stability for $\mathcal{T}_{sC}$ finally indicates that the unscreened Coulomb-modified p-d T matrix is obtained.

The spin scattering matrix M is then give in terms of the angular momentum recoupling coefficients:[24]

$$\langle \sigma_{\beta_z} j_{\beta_z}|M(\theta)|\sigma_{\alpha_z} j_{\alpha_z}\rangle = \delta_{\sigma_{\beta_z},\sigma_{\alpha_z}}\delta_{j_{\beta_z},j_{\alpha_z}} f_C(\theta)$$

$$- \sum_{JL_\beta L_\alpha}\sum_{S_\beta S_\alpha}\left[\frac{2L_\alpha+1}{4\pi}\right]^{1/2} Y_{L_\beta L_{\beta_z}}(\theta,0)$$

$$\times\langle \sigma_\alpha\sigma_{\alpha_z} j_\alpha j_{\alpha_z}|S_\beta S_{\beta_z}\rangle\langle \sigma_\beta\sigma_{\beta_z} j_\beta j_{\beta_z}|S_\alpha S_{\alpha_z}\rangle$$

$$\times\langle L_\beta L_{\beta_z} S_\beta S_{\beta_z}|JS_{\alpha_z}\rangle\langle L_\alpha 0 S_\alpha S_{\alpha_z}|JS_{\alpha_z}\rangle e^{i\sigma_{L_\beta}}\langle L_\beta S_\beta|\mathcal{T}^{J\pi I_z}_{sC}|L_\alpha S_\alpha\rangle e^{i\sigma_{L_\alpha}} . \quad (12)$$

Y_{lm} are the spherical harmonics, $f_C(\theta)$ is the Rutherford scattering amplitude, and σ_L denotes the Coulomb scattering phase shifts. The polarization observables are calculated from the M matrix according to the Madison Convention.[25]

Before demonstrating the convergence of the screening procedure on the level of *p-d* observables, we briefly address another convergence problem connected with the calculation of scattering observables. Since the summation over the number of three-nucleon total angular momenta J has to be finite in practice, the question where to terminate arises. At an energy of $E_{\rm lab}=2.5$ MeV we have found for *n-d* first-order polarization observables that $J=\frac{13}{2}$ is quite sufficient (Fig. 2). For observables other than vector analyzing powers convergence is even faster, and fewer partial waves would be sufficient.

Examples of the practicality of the screening and renormalization procedure for Coulomb-modified three-nucleon scattering are given in Fig. 3. At an energy of $E^N_{\rm lab}=3.0$ MeV differential cross sections, proton analyzing powers, and deuteron polarizations T_{20} are given for various values of the screening radius. It is obvious that numerical stability (i.e., the unscreened physical *p-d* quantity) can be seen for values less than 300 fm. The slowest convergence is found in A_y, which is linked with the fact that higher three-nucleon angular momenta are necessary, which implies a larger impact parameter in the scattering process and consequently less rigorous screening of the long-range Coulomb interaction. The *p-d* observables are calculated with the PEST16 potential, and experimental data[26–28] are shown for comparison. The results provide a reasonable description of the data on the average. However, we want to concentrate our calculations at a slightly lower energy of $E^N_{\rm lab}=2.5$ MeV because the data of A_y are more recent and we may avoid effects that can arise near the breakup threshold from our substitution of the Coulomb T matrix by the Coulomb potential.[14] At energies well above the breakup threshold the data would be better established, but the investment in coding work and computer time would be significantly increased compared to the already expensive *p-d* calculation of the present work. On the other hand, at such low energies only few *N-N* partial waves become important for *p-d* observables, thus providing a better test for differentiating between different *N-N* model parametrizations.

The results of our calculations at $E_{\rm lab}=2.5$ MeV with the PEST16 potential are shown in Fig. 4. We compare therein experimental data[29,30] with four different calculations, namely, *n-d*, *p-d*, *p-d* with neglect of the $l=1$ *N-N* partial waves and an approximate *p-d*.[31] The latter is based on the *n-d* result where the two-body Coulomb interaction between the proton and the electric charge located in the center of mass of the deuteron is added on.

Overall, the full *p-d* calculation yields results that are roughly compatible with the experimental data. Compared to the accuracy of the data the Coulomb distortion effect is not too big but nevertheless must not be neglected. In particular for the differential cross section and the tensor polarization T_{20} and T_{21} a correct treatment of the Coulomb corrections is suggested. As far as the nucleon analyzing power is concerned an interesting parallel is found to a situation given by experiments at higher energies, e.g.,e at $E_{\rm lab}=8$ MeV.[32] There, the experimental data of comparable accuracy display for neutron- and proton-analyzing powers, when fitted with Legendre polynomials, a very similar behavior in the maximum around $\theta_{\rm c.m}=110°$. As already found in Ref. 32 and in a calculation employing different approximate three-body Coulomb corrections[18] the simple approximate *p-d* of Ref. 31 fails to describe the measured difference in the maximum of A_y. Again, the exact *p-d* calculation has

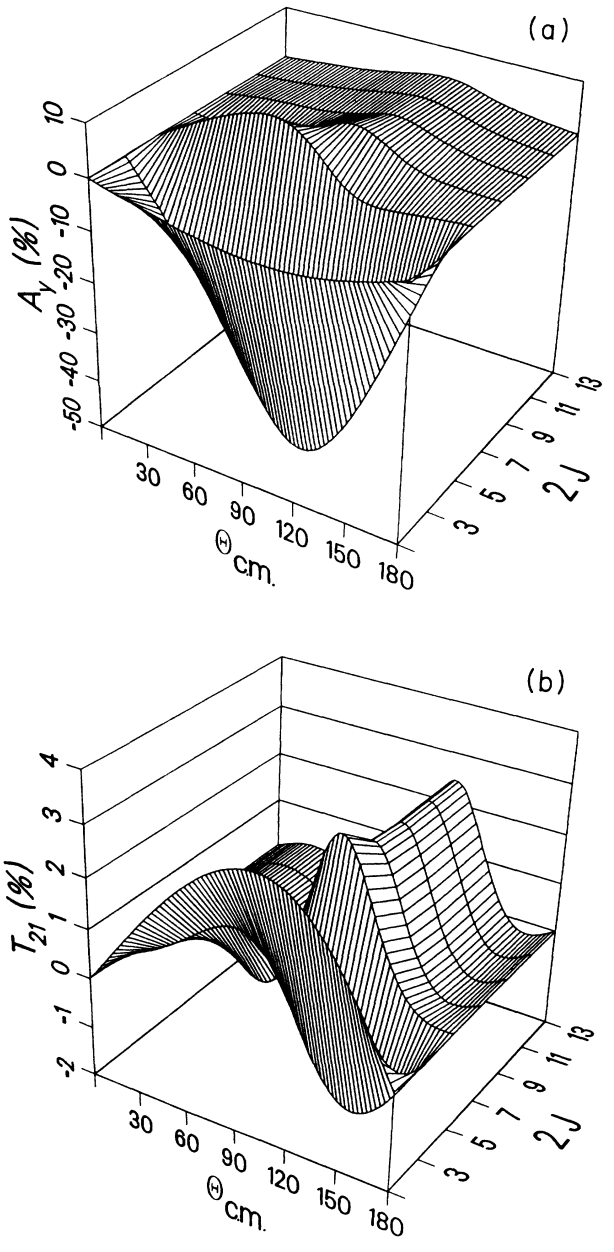

FIG. 2. Convergence of *n-d* first-order polarization observables as a function of the three-nucleon total angular momentum J. Shown are A_y and T_{21} calculated with the PEST16 potential.

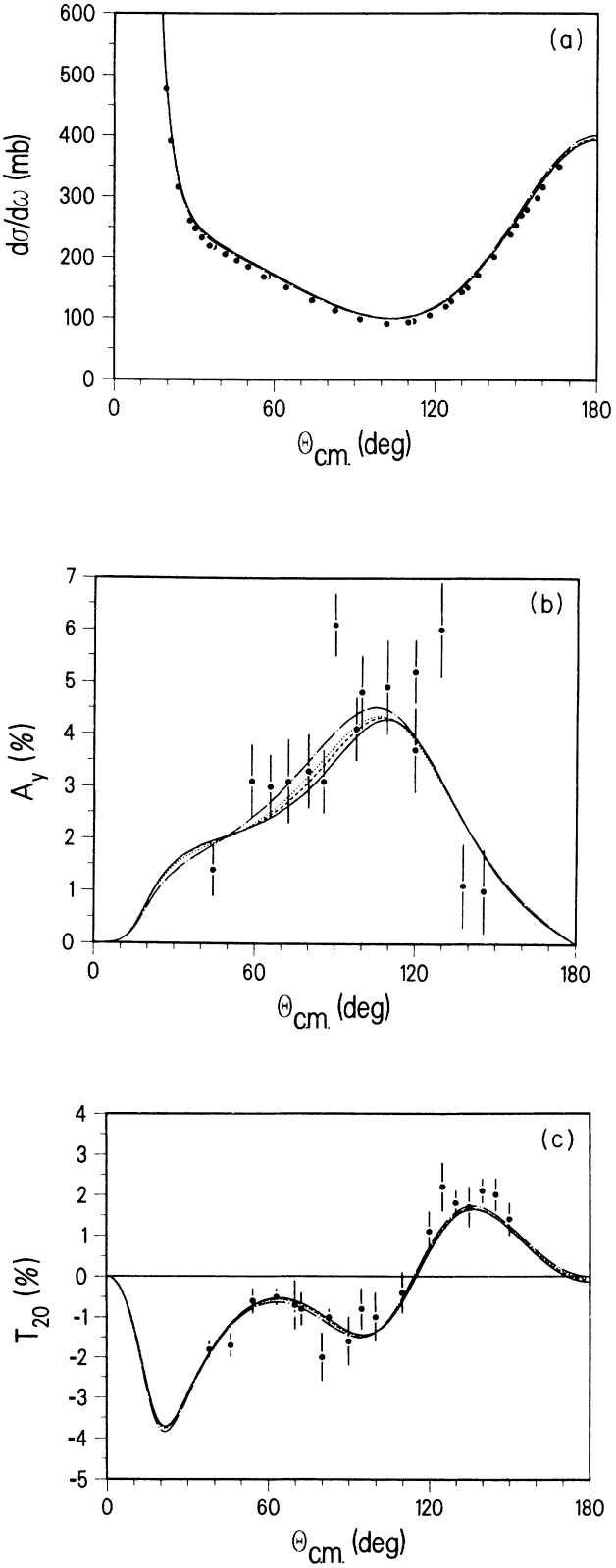

FIG. 3. Sample of *p-d* observables calculated with the PEST16 potential at $E_{\text{lab}}^{p}=3.0$ MeV for different values of the screening radius ($R=300$ fm: solid line; $R=100$ fm: dashed line; $R=50$ fm: dotted line; $R=10$ fm: dashed-dotted line). The data are from Refs. 26, 27, and 28 for $d\sigma/d\omega$, A_y, and T_{20}, respectively.

obviously to be invoked.

The *p-d* results without $l=1$ *N-N* partial waves demonstrate well-known features except in T_{20} and T_{21}, where the significant *P*-wave contributions disqualify the assumption that *N-N* tensor force governs the three-nucleon first-order tensor observables. The reason for this discrepancy could be that at smaller energies the importance of the lower partial waves (*P* states) relative to the *D*-state admixture in the $^3S_1$-$^3D_1$ tensor state is enhanced, whereas at higher energies the *D* state becomes increasingly important.

Since no *p-d* measurements for second-order polarization observables at energies below the breakup threshold are available, only a few examples of the numerous observables are given in cases where the Coulomb distortion effect is significant (Figs. 5–7).

To study the question of the model dependence of the Coulomb corrections we have performed three different sets of calculations with the potentials described in Sec. III. Although the PEST16 and the Yamaguchi-like potentials are not on-shell equivalent they display close similarity in the *N-N* lower-energy properties to allow a sensible comparison of the impact two distinctively different half-off-shell extensions on the Coulomb corrections in *p-d* scattering. In each of Figs. 8–13 three different cases are presented showing the model dependence of the Coulomb distortion corrections. Comparison of case (a) and (b) of each figure displays the influence of the different *N-N* *P*-wave potential models, whereas case (b) and (c) represent the influence of the different $^1S_0$ and $^3S_1$-$^3D_1$ potentials. This comparison shows, that the Coulomb corrections are hardly model dependent, at least in a qualitative sense. Consequently the better agreement of the results with the PEST16 potential is expected not to be plagued by uncertainties of model-dependent Coulomb corrections. We may interpret our results therefore in the following way: the PEST16 potential represents the properties of the *N-N* interaction at lower energies quite well, which can be seen in the low-energy *p-d* scattering observables that are mainly sensitive to low-energy, low-angular-momentum, *N-N* states. Shortcomings of the simple potential model in the mixing parameter and the *D* state of the coupled $^3S_1$-$^3D_1$ state at higher *N-N* scattering energies seem to be suppressed at such small three-nucleon scattering energies. Finally, the special insensitivity of T_{22} against *N-N* partial waves other than the $^3S_1$-$^3D_1$ state should be mentioned. Since the Coulomb corrections are very small, higher precision *p-d* data at low energies could provide a rather stringent test for the dominant *N-N* partial wave in this case.

V. PHASE SHIFTS

To uniquely determine phase shift parameters within a phase shift analysis a certain number of measured observables depending on the spins of the involved scattering particles has to be available. Since for *p-d* scattering a representation of the data at $E_{\text{lab}}=3.0$ MeV through phase parameters exists,[33] it is of interest to compare with phase parameters obtained from our solutions of the

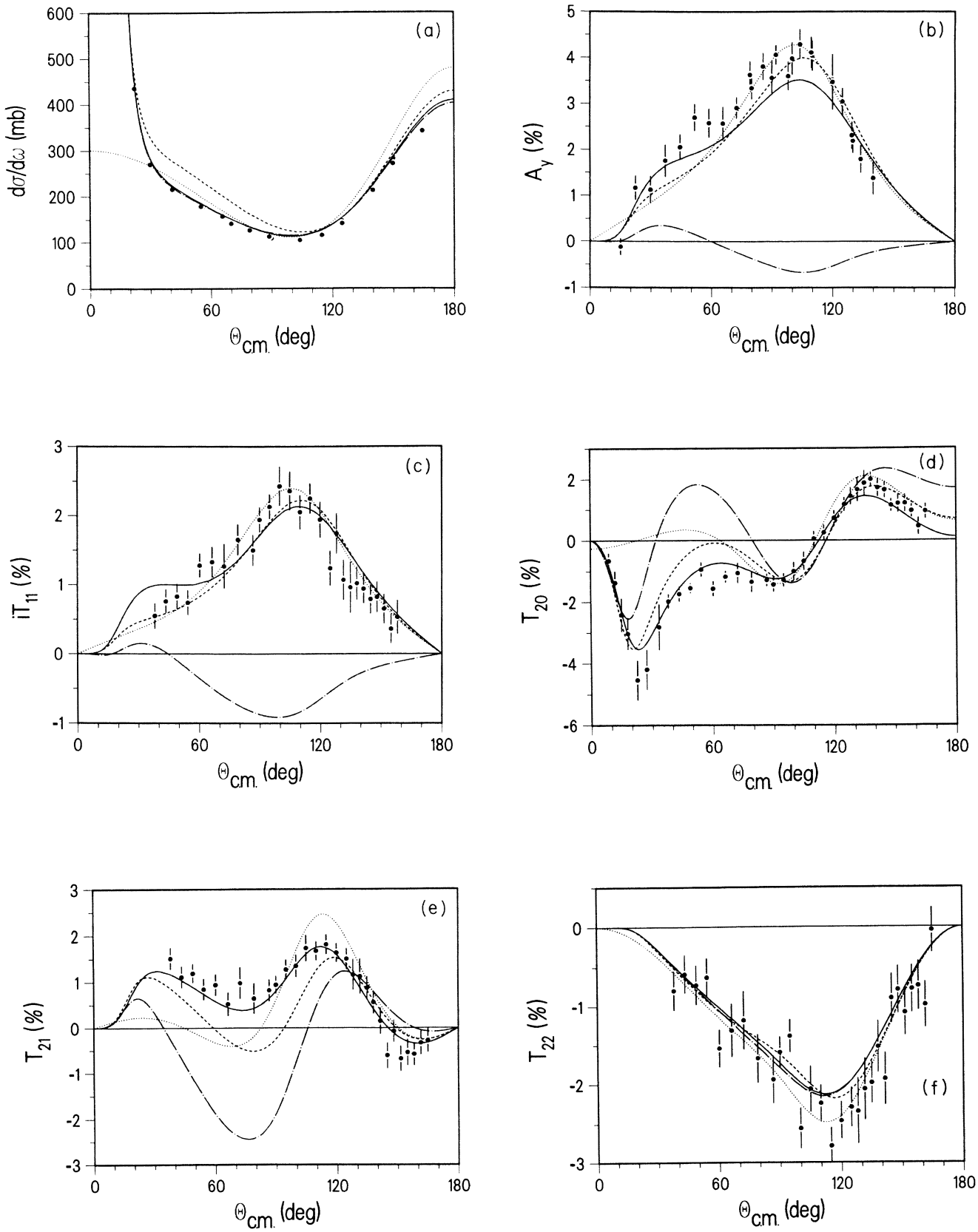

FIG. 4. *N-d* zero- and first-order polarization observables at $E_{\text{lab}}^{N}=2.5$ MeV calculated with the PEST16 potential. Four different computational results are shown: full *p-d* (solid line), *n-d* (dotted line), *p-d* without *N-N P* waves (dashed-dotted), and an approximate *p-d* on the basis of a very simple Coulomb correction (dashed line) (Ref. 31). The data for the differential cross section are from Ref. 29, whereas those of the first-order polarizations are from Ref. 30.

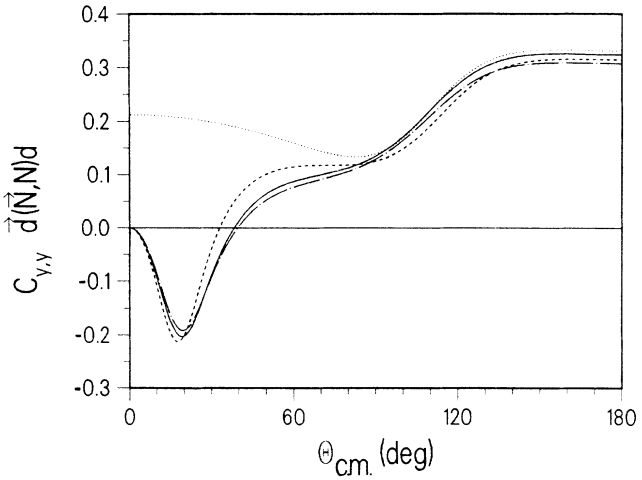

FIG. 5. Second-order N-d observables C_{yy} at $E_{\rm lab}^N = 2.5$ MeV. The notation is the same as in Fig. 4.

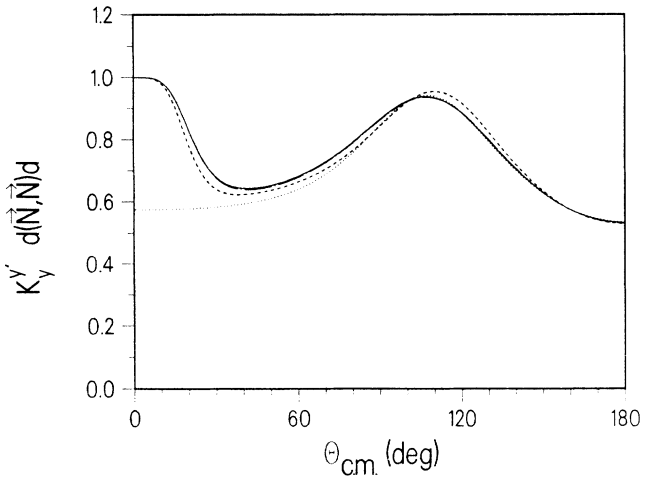

FIG. 6. Second-order N- d observable $K_y^{y'}$ at $E_{\rm lab}^N = 2.5$ MeV. The notation is the same as in Fig. 4.

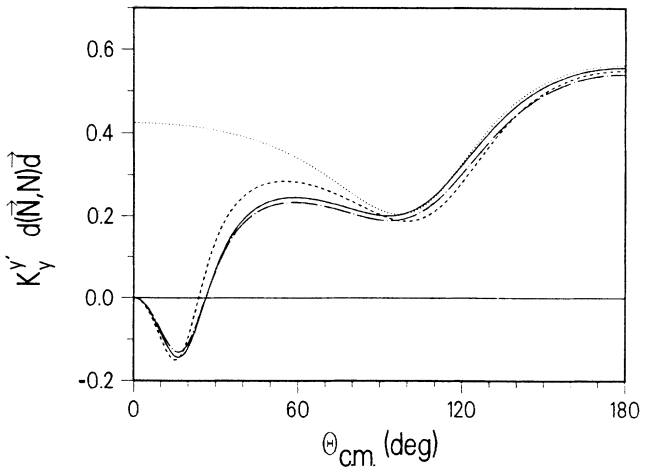

FIG. 7. Second-order N-d observable $K_y^{y'}$ at $E_{\rm lab}^N = 2.5$ MeV. The notation is the same as in Fig. 4.

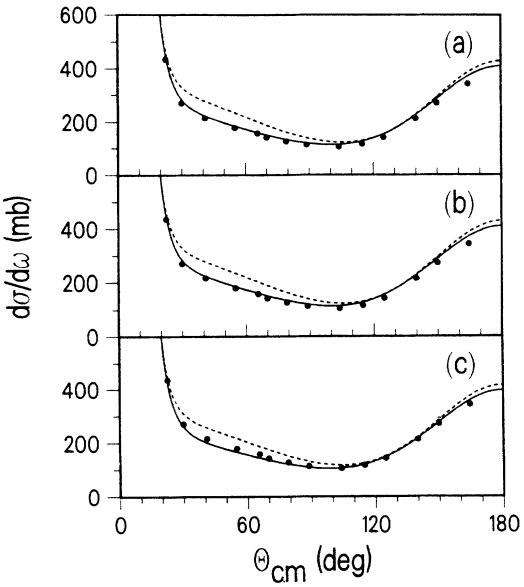

FIG. 8. p-d differential cross sections at $E_{\rm lab}^p = 2.5$ MeV. The result obtained with the PEST16 potential is shown at the top (a), (b) contains the result with PEST16 in the $^1S_0$ and $^3S_1$-$^3D_1$ state and the Y potentials in the P waves, and (c) shows the result with Y potentials. The notation is the same as in Fig. 4.

p-d scattering equations. We start with the three-body S matrix in its partial-wave decomposed form, which can easily be computed from the solutions of the Faddeev equations (on-shell T matrices) for every combination of the total angular momentum J and the parity π. This is a 3×3 (2×2) matrix for each $J \geq \frac{3}{2}$ ($J = \frac{1}{2}$). Therefore, the 6 (3) complex quantities can be parametrized in terms of

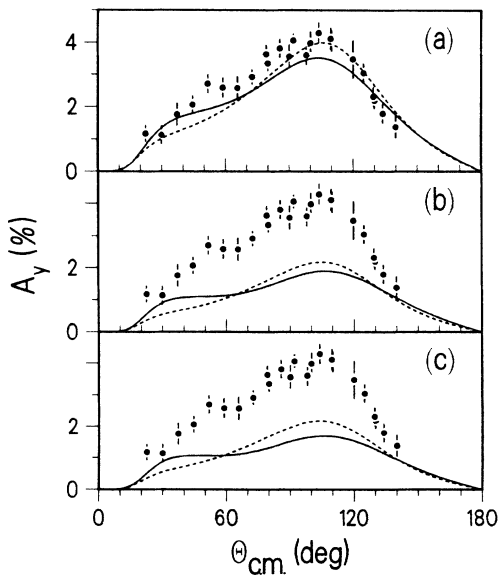

FIG. 9. p-d first-order polarization observable A_y at $E_{\rm lab}^p = 2.5$ MeV. The notation is the same as in Fig. 8.

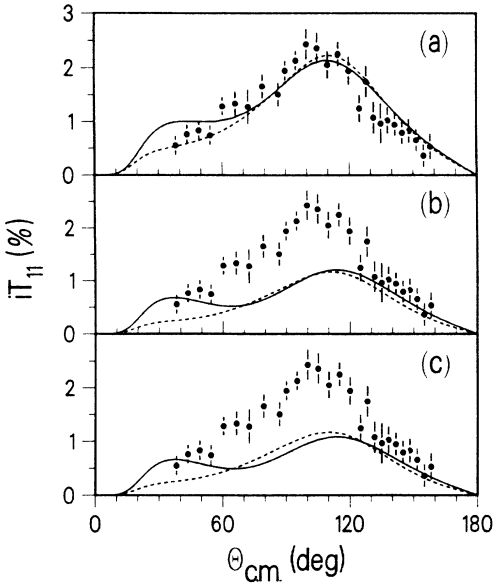

FIG. 10. *p-d* first-order polarization observable iT_{11} at $E^p_{lab}=2.5$ MeV. The notation is the same as in Fig. 8.

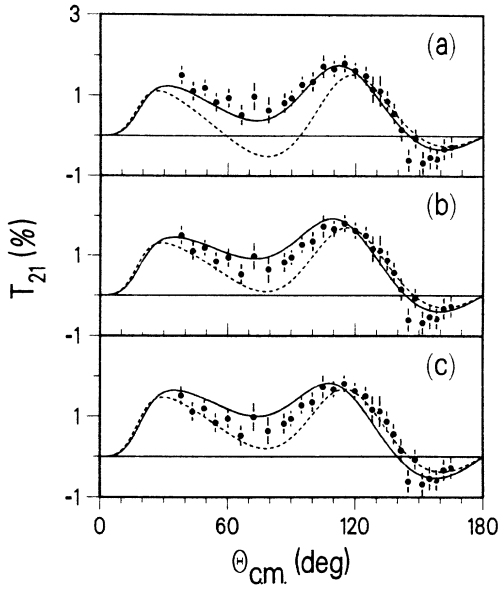

FIG. 12. *p-d* first-order polarization observable T_{21} at $E^p_{lab}=2.5$ MeV. The notation is the same as in Fig. 8.

3 (2) complex phase shifts and 3 (1) complex mixing parameters:[34]

$$S^{J\pi}=u^{J\pi\dagger}\exp(2i\delta^{J\pi})u^{J\pi}\ . \tag{13}$$

δ stands for a diagonal phase shift matrix and the matrix u describes the three successive *Blatt and Biedenharn rotations* about the mixing parameters ϵ, η, and ζ. For energies below the breakup threshold these phase parameters remain real quantities thus halving the number of parameters.

It is interesting to note that the solution of the preceding equation leaves us with the freedom to reorder the phase shifts, depending on the ordering of the states in the angular momentum coupling scheme. We solve Eq. (13) and make permutations of the eigenphase shifts corresponding to the following assumptions about their arrangement: For each total angular momentum we assume that the first phase belongs to the quartet state with the lowest possible angular momentum. The second one is assigned to the second quartet state and the third to the doublet state. No further rearrangements of the phase shifts or the mixing parameters are performed. This procedure yields the opposite sign for the mixing parameters ϵ and η compared to Ref. 35.

In Table III we first show the results of the phase shift representation of our different *n-d* scattering calculation-

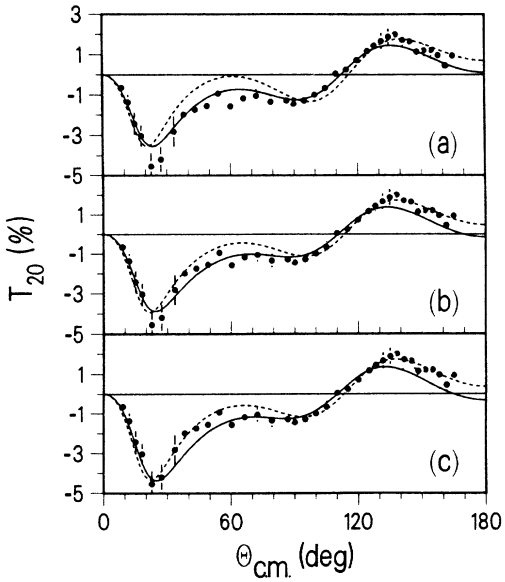

FIG. 11. *p-d* first-order polarization observable T_{20} at $E^p_{lab}=2.5$ MeV. The notation is the same as in Fig. 8.

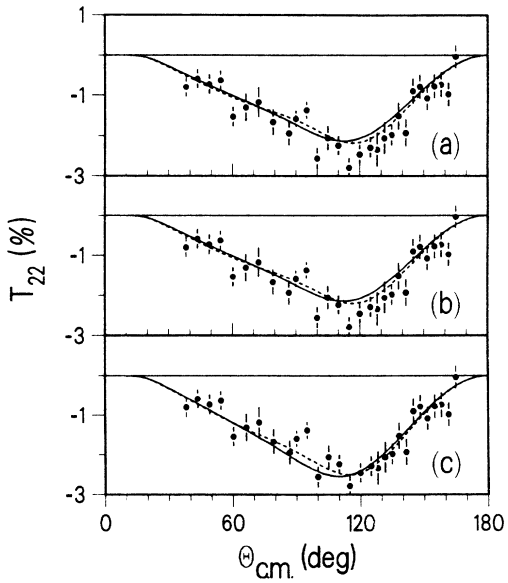

FIG. 13. *p-d* first-order polarization observable T_{22} at $E^p_{lab}=2.5$ MeV. The notation is the same as in Fig. 8.

al results at $E^p_{lab}=2.5$ MeV. Due to the almost blank *n-d* data base at this energy, no phase shift analysis exists and we may compare with other theoretical results at most. Unfortunately, at exactly the energy considered here this comparison is not quite possible and we may only point out that the results obtained by Lamot *et al.*[36] for a nearby energy of $E^n_{lab}=3.0$ MeV are roughly similar, where comparable potentials like the Yamaguchi-type potential were used.

The change of the strong interaction in the $^1S_0$ and the coupled $^3S_1$-$^3D_1$ *N-N* state influences mostly the three-body *S* waves and the mixing between the two states of $J^\pi=\frac{1}{2}^+$. A strong dependence of the $J^\pi=\frac{1}{2}^-$ states on the *N-N* waves is also transparent. A similar observation can be made in the other quartet three-body *P* states. A manifestation of *N-N* $l=1$ state influence is also found in the mixing parameters $\epsilon^{1/2-}$ and $\epsilon^{3/2-}$. There are only two cases with stronger dependence from the *N-N* potential model and in particular from the half-shell behavior, namely the $^4P_{1/2}$ and the $^2S_{1/2}$ where the *N-N P*, respectively, *S* waves play a role.

Next Table IV shows our results for the Coulomb-modified strong *p-d* phase shifts at $E^p_{lab}=2.5$ MeV. The results contained in Table III together with the one of Table IV provide information on the Coulomb distortion corrections and their model dependence on the level of phase shifts. Our Coulomb corrections display a similar trend as was found previously by Alt *et al.*[37] although for unsplit phase shifts that were calculated using *N-N S* waves only and with one potential model solely. Except for the $^2S_{1/2}$ phase shift the Coulomb corrections are hardly model dependent, which we already have seen at the level of the first-order polarization observables (Sec. IV), where the $^2S_{1/2}$ state does not significantly contribute to the angular distribution in first-order polarization.

Table IV also contains the results of a phase shift analysis performed by Schmelzbach *et al.*[33] at $E^p_{lab}=3.0$ MeV together with computational results obtained with the PEST16 potential. Apart from the sign change in the ϵ and η parameter a rough similarity in the phase parameters is given, but the differences in magnitude are in some cases significant. The doublet phases seem to be quite small in the phase shift analysis[38] and in the $J^\pi=\frac{5}{2}^-$ state the doublet *F* wave seems to acquire a rather large value at the expense of nonexisting mixing parameters. A similar situation is given in $J^\pi=\frac{5}{2}^+$ state where η and ζ seem to be zero at the expense of a bigger quartet *D* wave and ϵ-mixing parameter. We therefore conclude that an immediate comparison of the experimental and theoretical results might not be very informa-

TABLE III. *n-d* phase parameters (deg).

Potential used in $^1S_0$, $^3S_1$-$^3D_1$ *P* states	PEST16	*Y*5.5%	PEST16 PEST16	PEST16 *Y* type	*Y*5.5% *Y* type
$^2P_{1/2}$	−6.44	−6.28	−7.09	−6.94	−6.78
$^4P_{1/2}$	19.15	18.45	21.81	22.89	22.09
$\epsilon^{1/2-}(^2P_{1/2}$-$^4P_{1/2})$	−3.08	−3.20	−5.24	−5.89	−6.02
$^2S_{1/2}$	−36.13	−28.19	−35.74	−35.84	−28.59
$^4D_{1/2}$	−3.26	−3.18	−3.24	−3.21	−3.14
$\eta^{1/2+}(^2S_{1/2}$-$^4D_{1/2})$	−0.57	−1.01	−0.50	−0.46	−0.84
$^4F_{3/2}$	0.71	0.70	0.71	0.71	0.70
$^2P_{3/2}$	−6.43	−6.27	−6.89	−6.79	−6.63
$^4P_{3/2}$	27.52	26.84	24.90	24.59	23.96
$\epsilon^{3/2-}(^2P_{3/2}$-$^4P_{3/2})$	0.96	1.04	2.06	2.07	2.12
$\zeta^{3/2-}(^4F_{3/2}$-$^4P_{3/2})$	0.39	0.40	0.34	0.34	0.34
$\eta^{3/2-}(^4F_{3/2}$-$^2P_{3/2})$	−2.94	−3.06	−2.78	−2.84	−2.95
$^4S_{3/2}$	−66.06	−65.35	−66.01	−65.96	−65.25
$^2D_{3/2}$	1.97	1.93	1.95	1.96	1.93
$^4D_{3/2}$	−3.49	−3.43	−3.49	−3.48	−3.41
$\epsilon^{3/2+}(^4S_{3/2}$-$^4D_{3/2})$	−0.64	−0.64	−0.50	−0.41	−0.41
$\zeta^{3/2+}(^4S_{3/2}$-$^2D_{3/2})$	−1.22	−1.27	−1.30	−1.34	−1.38
$\eta^{3/2+}(^4S_{3/2}$-$^2D_{3/2})$	−0.35	−0.36	−0.40	−0.42	−0.44
$^4P_{5/2}$	22.44	21.66	24.43	24.23	23.45
$^2F_{5/2}$	−0.36	−0.36	−0.36	−0.36	−0.36
$^4F_{5/2}$	0.74	0.73	0.74	0.74	0.73
$\epsilon^{5/3-}(^2F_{5/2}$-$^4F_{5/2})$	−0.47	−0.47	−0.48	−0.50	−0.51
$\zeta^{5/2-}(^4P_{5/2}$-$^4F_{5/2})$	−0.99	−1.03	−0.92	−0.91	−0.95
$\eta^{5/2-}(^4P_{5/2}$-$^2F_{5/2})$	−0.35	−0.37	−0.33	−0.32	−0.34
$^4G_{5/2}$	−0.15	−0.15	−0.15	−0.15	−0.15
$^2D_{5/2}$	1.94	1.90	1.92	1.93	1.89
$^4D_{5/2}$	−3.77	−3.71	−3.78	−3.78	−3.72
$\epsilon^{5/2+}(^2D_{5/2}$-$^4D_{5/2})$	0.30	0.30	0.22	0.22	0.22
$\zeta^{5/2+}(^4G_{5/2}$-$^4D_{5/2})$	0.61	0.63	0.62	0.62	0.63
$\eta^{5/2+}(^4G_{5/2}$-$^2D_{5/2})$	−1.84	−1.90	−1.85	−1.84	−1.90

TABLE IV. *p-d* phase parameters (deg).

Potential used in $^1S_0$, $^3S_1$-$^3D_1$			PEST16	PEST16	*Y*5.5%	PEST16	Expt.
P states	PEST16	*Y*5.5%	PEST16	*Y* type	*Y* type	PEST16	Ref. 33
$E_{\rm lab}^p$ (MeV)	2.5	2.5	2.5	2.5	2.5	3.0	3.0
$^2P_{1/2}$	−6.45	−6.33	−7.01	−6.86	−6.75	−7.34	−3.39
$^4P_{1/2}$	17.16	16.54	19.36	20.25	19.52	23.56	22.70
$\epsilon^{1/2-}(^2P_{1/2}$-$^4P_{1/2})$	−2.69	−2.83	−4.58	−5.15	−5.22	−6.05	6.08
$^2S_{1/2}$	−31.95	−21.54	−31.32	−31.46	−21.91	−38.75	−23.69
$^4D_{1/2}$	−3.03	−2.96	−3.02	−2.99	−2.93	−3.85	−4.26
$\eta^{1/2+}(^2S_{1/2}$-$^4D_{1/2})$	−0.71	−1.58	−0.64	−0.58	−1.31	−0.41	6.79
$^4F_{3/2}$	0.59	0.58	0.59	0.59	0.58	0.93	0.85
$^2P_{3/2}$	−6.44	−6.32	−6.86	−6.76	−6.64	−7.07	−2.18
$^4P_{3/2}$	24.40	23.76	22.16	21.85	21.30	26.41	22.98
$\epsilon^{3/2-}(^2P_{3/2}$-$^4P_{3/2})$	0.86	0.90	1.79	1.79	1.80	2.42	−3.19
$\zeta^{3/2-}(^4F_{3/2}$-$^4P_{3/2})$	0.41	0.42	0.37	0.37	0.38	0.35	
$\eta^{3/2-}(^4F_{3/2}$-$^2P_{3/2})$	−2.60	−2.69	−2.46	−2.52	−2.60	−3.46	
$^4S_{3/2}$	−58.94	−58.29	−58.88	−58.85	−58.20	−70.17	−68.57
$^2D_{3/2}$	1.65	1.63	1.64	1.65	1.62	2.35	0.70
$^4D_{3/2}$	−3.26	−3.19	−3.25	−3.24	−3.18	−4.16	−4.68
$\epsilon^{3/2+}(^2D_{3/2}$-$^4D_{3/2})$	−0.74	−0.75	−0.61	−0.52	−0.53	−0.46	0.70
$\zeta^{3/2+}(^4S_{3/2}$-$^4D_{3/2})$	−1.19	−1.24	−1.27	−1.30	−1.35	−1.54	−0.40
$\eta^{3/2+}(^4S_{3/2}$-$^2D_{3/2})$	−0.30	−0.31	−0.35	−0.36	−0.38	−0.50	0.59
$^4P_{5/2}$	20.01	19.32	21.74	21.55	20.78	26.29	24.26
$^2F_{5/2}$	−0.38	−0.38	−0.38	−0.38	−0.38	−0.47	−1.65
$^4F_{5/2}$	0.61	0.60	0.61	0.61	0.60	0.96	0.85
$\epsilon^{5/2-}(^2F_{5/2}$-$^4F_{5/2})$	−0.30	−0.30	−0.31	−0.33	−0.34	−0.49	
$\zeta^{5/2-}(^4P_{5/2}$-$^4F_{5/2})$	−0.99	−1.03	−0.92	−0.92	−0.96	−1.06	
$\eta^{5/2-}(^4P_{5/2}$-$^2F_{5/2})$	−0.35	−0.37	−0.33	−0.33	−0.34	−0.39	
$^4G_{5/2}$	−0.17	−0.17	−0.17	−0.17	−0.17	−0.21	−0.34
$^2D_{5/2}$	1.63	1.60	1.62	1.62	1.59	2.31	−1.67
$^4D_{5/2}$	−3.51	−3.45	−3.52	−3.52	−3.46	−4.53	−5.47
$\epsilon^{5/2+}(^2D_{5/2}$-$^4D_{5/2})$	0.36	0.36	0.28	0.28	0.28	0.20	−1.67
$\zeta^{5/2+}(^4G_{5/2}$-$^4D_{5/2})$	0.62	0.64	0.62	0.62	0.64	0.72	
$\eta^{5/2+}(^4G_{5/2}$-$^2D_{5/2})$	−1.97	−2.03	−1.98	−1.97	−2.04	−2.13	

tive. However, our results could provide guidance for a new run of the phase shift analysis that would also include the existing data at $E_{\rm lab}^p = 2.5$ MeV.

VI. APPROXIMATE COULOMB CORRECTIONS

Given the fact that a correct treatment of the Coulomb interaction in *p-d* scattering requires a lot of man-hours and computer time, it is legitimate to search for acceptable approximations. In Sec. IV it was already demonstrated that a very simple approximation[31] completely failed. On the other hand, our calculations have indicated that the three-nucleon Coulomb distortion corrections are scarcely influenced by the details of the model used for the *N-N* interaction. It is therefore appropriate to study an existing model-independent approximation of the Coulomb distortion corrections, which has already been applied for a description of *p-d* polarization observables.[39] The basic idea therein was to start with the on-shell strong three-nucleon *T* matrix derived with an arbitrary *N-N* interaction model or by *n-d* phase shift analysis, if available, and to then approximate the external part of the Coulomb corrections, i.e., the Coulomb wave function, in a two-body manner.

The simple formula for the approximate Coulomb-modified reactance matrix Q_{sC}, which is related to the transition matrix by $T = Q(1-iQ)^{-1}$, reads

$$Q_{sC,\beta\alpha}(q) = Q_{s,\beta\alpha}(q) - \delta_{\beta\alpha}\frac{\pi}{2}\bar{v}_{C,\alpha}(q) + \frac{\eta}{\pi}[c_\beta(q)+c_\alpha(q)][Q_{s,\beta\alpha}(q)+q\frac{d}{dq}Q_{s,\beta\alpha}(q)] \ . \tag{14}$$

$\bar{v}_C$ is the difference of the full electromagnetic potential and the point-like Coulomb potential between the proton and the deuteron. The approximation of the Coulomb wave function includes the model-independent quantities

$$c_\alpha(q) = \int_0^{P_\infty} \frac{x^2 dx}{1-x^2} \int_{-1}^{1} \frac{dy\, P_{L_\alpha}(y) f[q^2(1+x^2-2xy)]}{1+x^2-2xy} \ , \qquad \eta = \mu e^2/q \tag{15}$$

and the energy derivation of Q_s. P_l denotes the Legendre polynomial and $f(p)$ is the form factor for the (spherical) charge distribution of the deuteron.

Inserting the Q_s as given by our *n-d* calculation with the PEST16 potential at $E_{\rm lab}^n$ between 0.5 and 3.0 MeV we obtain Q_{sC} and hence approximate *p-d* observables that can be compared with our exact *p-d* results. In Fig. 14 the first-order polarization observables at $E_{\rm lab}^p = 2.5$

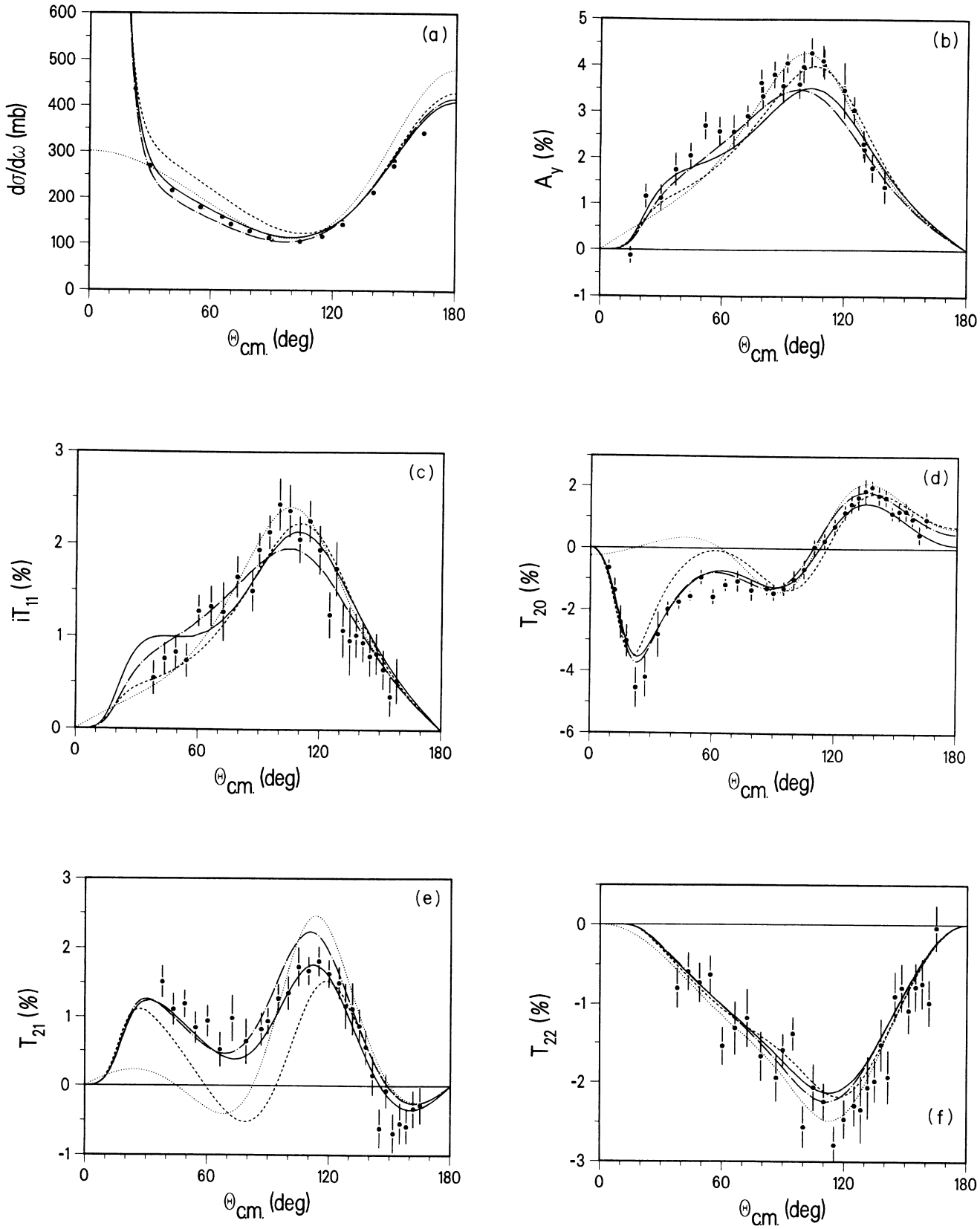

FIG. 14. *N-d* first-order polarization observables at $E_{\text{lab}}^{N}=2.5$ MeV calculated with the PEST16 potential. The full *p-d* calculation (solid line) is compared with the results obtained using the OSA (dashed-dotted line) and using the simplest approximate Coulomb correction of Ref. 31 (dashed line). The dotted line denotes the corresponding *n-d* result. The data are from Ref. 30.

MeV calculated with this on-shell approximation (OSA) are shown together with the exact *p-d*, the simple *p-d* approximation of Ref. 31, and the *n-d* result. Apart from the angular region around 120 deg in T_{21} the OSA results represent a fair approximation and are indeed consistently superior to the simple approximation,[31] where the Coulomb distortion had been neglected completely. A similar situation is given for the spin correlation parameters of the reaction $\mathbf{d}(\mathbf{p},p)d$.

If the OSA approximation would work equally well at other energies; in particular at higher energies above the breakup threshold a computationally inexpensive and sufficiently accurate method would be at hand to analyze the abundant *p-d* data basis starting with the most elaborate *n-d* calculations that are available, such as the one of Glöckle *et al.* with the Bonn or Paris potential.[40] However, it has been argued by Alt *et al.*[37] that such effective two-body on-shell approximation will run into trouble at higher energies. A final word on this question may therefore be said only when exact *p-d* calculations with higher *N-N* partial waves at energies above the breakup threshold have been carried out.

VII. SUMMARY

In this paper, Coulomb-modified Faddeev equations in momentum space are presented and, for the first time, allow the inclusion of *N-N* partial waves other than *S* states. The full spin-isospin partial-wave decomposed coupled integral equations are solved by employing the screening method for the Coulomb potential and it is demonstrated in a numerical way that the *p-d* observables stabilize for screening radii of up to a worst-case limit of 300 fm. At an energy of $E_{\rm lab}^N = 2.5$ MeV it is shown that the transition matrix has to be summed up to $J = \frac{13}{2}$ to obtain converged observables.

Our calculations with two sets of *N-N* potentials that behave rather similarly at smaller *N-N* scattering energies but quite differently off the energy shell demonstrate that the three-nucleon Coulomb corrections must not be neglected at this energy and that they are hardly model dependent. The PEST16 potential, which is a separable rank-one representation of the Paris potential, consistently yields a rather close description of the measured *p-d* zero-and first-order polarization observables in contrast to the potential of the usual one-term Yamaguchi type. At the small three-nucleon energy we have performed our calculations of the lower-energy *N-N* scattering phase shifts in low *N-N* states, and the static properties of the deuteron seem to be most important since both aspects are well reproduced by the PEST16 potential. Higher-accuracy *p-d* polarization measurements at low three-nucleon energy could provide a more stringent test of these few features of the *N-N* interaction, in particular a T_{22} measurement for the $^3S_1$-$^3D_1$ tensor channel. Second-order polarization observables are also calculated and significant Coulomb corrections are found in some of these quantities, but unfortunately no measurements are available at these low energies.

On the basis of phase shifts we are able to trace back the influence of different *N-N* on three-nucleon states. A comparison with *p-d* phase shift analysis reveals some differences which might inspire new activities for *p-d* phase shift analysis towards including smaller energies.

Finally, we make use of an approximate effective two-body description of the three-nucleon Coulomb corrections and find that at $E_{\rm lab}^N = 2.5$ MeV the approximation performs quite well compared to the expensive exact *p-d* calculation. Whether such a simple method could replace the full and time consuming treatment at other higher energies cannot be judged at the moment.

ACKNOWLEDGMENTS

The authors would like to thank W. Grüebler for communicating the experimental details, N. Gee and the OPAL group (CERN) for access to their computer facilities, C. Chandler for providing valuable comments, and the Fonds zur Förderung der wissenshaftlichen Forschung in Österreich, Projects No. 5797 and J0312P for support. G. H. Berthold and H. Zankel would also like to thank the University of New Mexico for its hospitality.

APPENDIX

The effective potential is a sum over four terms, whose graphical representations can be found in Refs. 1 and 2:

$$\mathcal{V}^{J\pi I_z}_{N_\beta N_\alpha}(q_\beta,q_\alpha;E) = \langle \mathbf{q}_\beta | \langle \bar{g}_\beta | \bar{\delta}_{\beta\alpha} + \bar{\delta}_{\beta 3}\bar{\delta}_{\alpha 3} G_0(E) v_C^R G_0(E) | \bar{g}_\alpha \rangle | \mathbf{q}_\alpha \rangle$$

$$= \sum_{k=a,b,c,d} V^{J\pi I_z(k)}_{N_\beta N_\alpha}(q_\beta,q_\alpha;E) \ . \tag{A1}$$

The term (a) describes only the strong interaction (*n-d* scattering) whereas part (b) takes into account the Coulomb interaction in the initial and final states. Their isospin representation reads as

$$V^{J\pi I_z(a,b)}_{N_\beta N_\alpha}(q_\beta,q_\alpha;E)$$

$$= \sum_{i_{\alpha_z} i_{\beta_z}} \hat{I}_\alpha \hat{I}_\beta \hat{i}_\alpha \hat{i}_\beta (-1)^{i_\beta + i_\alpha + i_{\beta_z} + i_{\alpha_z}} \begin{Bmatrix} \frac{1}{2} & i_\beta & I_\beta \\ I_z - i_{\beta_z} & i_{\beta_z} & -I_z \end{Bmatrix}$$

$$\times \begin{Bmatrix} \frac{1}{2} & \frac{1}{2} & i_\beta \\ i_{\alpha_z} + i_{\beta_z} - I_z & I_z - i_{\alpha_z} & -i_{\beta_z} \end{Bmatrix} \begin{Bmatrix} \frac{1}{2} & \frac{1}{2} & i_\alpha \\ I_z - i_{\beta_z} & i_{\alpha_z} + i_{\beta_z} - I_z & -i_{\alpha_z} \end{Bmatrix} \begin{Bmatrix} \frac{1}{2} & i_\alpha & I_\alpha \\ I_z - i_{\alpha_z} & i_{\alpha_z} & -I_z \end{Bmatrix} \tilde{V}^{J\pi I_z(a,b)}_{N_\beta N_\alpha}(q_\beta,q_\alpha;E) \; ; \tag{A2}$$

and correspondingly the Coulomb exchange graph (c) and the direct Coulomb graph (d):

$$V^{J\pi I_z(c,d)}_{N_\beta N_\alpha}(q_\beta,q_\alpha;E)$$

$$= \sum_{i_{\alpha_z} i_{\beta_z}} 3\hat{I}_\alpha \hat{I}_\beta \hat{i}_\alpha \hat{i}_\beta (-1)^{i_\beta + i_\alpha + i_{\beta_z} + i_{\alpha_z}} \begin{Bmatrix} \frac{1}{2} & i_\beta & I_\beta \\ I_z - i_{\beta_z} & i_{\beta_z} & -I_z \end{Bmatrix}$$

$$\times \begin{Bmatrix} \frac{1}{2} & \frac{1}{2} & i_\beta \\ i_{\alpha_z} + i_{\beta_z} - I_z & I_z - i_{\alpha_z} & -i_{\beta_z} \end{Bmatrix} \begin{Bmatrix} \frac{1}{2} & \frac{1}{2} & i_\alpha \\ I_z - i_{\beta_z} & i_{\alpha_z} + i_{\beta_z} - I_z & -i_{\alpha_z} \end{Bmatrix}$$

$$\times \begin{Bmatrix} \frac{1}{2} & i_\alpha & I_\alpha \\ I_z - i_{\alpha_z} & i_{\alpha_z} & -I_z \end{Bmatrix} \begin{Bmatrix} \frac{1}{2} & \frac{1}{2} & 1 \\ I_z - i_{\alpha_z} & I_z - i_{\beta_z} & -1 \end{Bmatrix}^2 \tilde{V}^{J\pi I_z(c,d)}_{N_\beta N_\alpha}(q_\beta,q_\alpha;E) \; . \tag{A3}$$

The symbol $\hat{j}$ is given by $\hat{j}=(2j+1)^{1/2}$. For rank-one N-N partial waves with arbitrary l we obtain for the effective po-

$$\tilde{V}^{J\pi I_z(\alpha)}_{N_\beta N_\alpha}(q_\beta,q_\alpha;E) = \sum_{\substack{l_\beta l_\alpha \\ aa'\mathcal{L}}} S^{(a)}_{N_\beta N_\alpha \mathcal{L} a a'} q_\beta^{a+a'} q_\alpha^{l_\alpha + l_\beta - a - a'} B^{(a)\mathcal{L}}_{n_\beta n_\alpha}(q_\beta,q_\alpha;E) \; , \tag{A4}$$

$$B^{(a)\mathcal{L}}_{n_\beta n_\alpha}(q_\beta,q_\alpha;E) = \tfrac{1}{2} \int_{-1}^{+1} d(\hat{\mathbf{q}}_\alpha \cdot \hat{\mathbf{q}}_\beta) P_{\mathcal{L}}(\hat{\mathbf{q}}_\alpha \cdot \hat{\mathbf{q}}_\beta) \frac{|-\frac{1}{2}\mathbf{q}_\beta - \mathbf{q}_\alpha|^{-l_\beta} g^*_{n_\beta}(|-\frac{1}{2}\mathbf{q}_\beta - \mathbf{q}_\alpha|) g_{n_\alpha}(|\frac{1}{2}\mathbf{q}_\alpha + \mathbf{q}_\beta|) |\frac{1}{2}\mathbf{q}_\alpha + \mathbf{q}_\beta|^{-l_\alpha}}{E - q_\alpha^2 - q_\beta^2 - \mathbf{q}_\alpha \cdot \mathbf{q}_\beta} \tag{A5}$$

$n_\alpha = \{l_\alpha, s_\alpha, j_\alpha, i_\alpha, i_{\alpha_z}\}$ denote the quantum numbers necessary to describe the two-nucleon state and $P_l(\cos\theta)$ are the Legendre polynomials.

$$S^{(\alpha)}_{N_\beta N_\alpha \mathcal{L} a a'} = \hat{L}_\beta \hat{L}_\alpha \hat{S}_\beta \hat{S}_\alpha \hat{j}_\beta \hat{j}_\alpha \hat{s}_\beta \hat{s}_\alpha \hat{l}_\beta \hat{l}_\alpha \hat{\mathcal{L}}^2 \left[\frac{(2l_\beta+1)!(2l_\alpha+1)!}{(2a)!(2a')!(2l_\beta-2a)!(2l_\alpha-2a')!} \right]^{1/2}$$

$$\times (\tfrac{1}{2})^{a-a'+l_\alpha} \sum_{\Lambda\Lambda' f} (-1)^R \hat{\Lambda}^2 \hat{\Lambda}'^2 \hat{f}^2 \begin{Bmatrix} a & a' & \Lambda' \\ 0 & 0 & 0 \end{Bmatrix} \begin{Bmatrix} \Lambda' & \mathcal{L} & L_\beta \\ 0 & 0 & 0 \end{Bmatrix}$$

$$\times \begin{Bmatrix} l_\beta - a & l_\alpha - a' & \Lambda \\ 0 & 0 & 0 \end{Bmatrix} \begin{Bmatrix} \Lambda & \mathcal{L} & L_\alpha \\ 0 & 0 & 0 \end{Bmatrix} \begin{Bmatrix} L_\alpha & L_\beta & f \\ \Lambda' & \Lambda & \mathcal{L} \end{Bmatrix} \begin{Bmatrix} S_\alpha & S_\beta & f \\ L_\beta & L_\alpha & J \end{Bmatrix}$$

$$\times \begin{Bmatrix} l_\alpha & l_\beta & f \\ a' & a & \Lambda' \\ l_\alpha - a' & l_\beta - a & \Lambda \end{Bmatrix} \begin{Bmatrix} f & l_\beta & l_\alpha & s_\alpha \\ S_\beta & j_\beta & \sigma_\beta & \sigma_\alpha \\ S_\alpha & s_\beta & j_\alpha & \sigma_\gamma \end{Bmatrix} ,$$

$$R = J - L_\alpha - L_\beta + S_\alpha + S_\beta - j_\alpha - j_\beta + \mathcal{L} - f + s_\beta - l_\beta + \tfrac{1}{2} \; . \tag{A6}$$

For the graph (b) we get

$$\tilde{V}^{J\pi I_z(b)}_{N_\beta N_\alpha}(q_\beta,q_\alpha;E) = \sum_{\substack{l_\beta l_\alpha \\ aa'\mathcal{L}}} S^{(a)}_{N_\beta N_\alpha \mathcal{L} a a'} q_\beta^{a+a'} q_\alpha^{l_\alpha + l_\beta - a - a'} B^{(b)\mathcal{L}}_{n_\beta n_\alpha}(q_\beta,q_\alpha;E) \; , \tag{A7}$$

with

$$B^{(b)\mathcal{L}}_{n_\beta n_\alpha}(q_\beta,q_\alpha;E)=\tfrac{1}{2}\int_{-1}^{+1}d(\hat{\mathbf{q}}_\alpha\cdot\hat{\mathbf{q}}_\beta)P_{\mathcal{L}}(\hat{\mathbf{q}}_\alpha\cdot\hat{\mathbf{q}}_\beta)\frac{|-\frac{1}{2}\mathbf{q}_\beta-\mathbf{q}_\alpha|^{-l_\beta}g^{R*}_{n_\beta}(|-\frac{1}{2}\mathbf{q}_\beta-\mathbf{q}_\alpha|)g_{n_\alpha}(|\frac{1}{2}\mathbf{q}_\alpha+\mathbf{q}_\beta|)|\frac{1}{2}\mathbf{q}_\alpha+\mathbf{q}_\beta|^{-l_\alpha}}{E-q_\alpha^2-q_\beta^2-\mathbf{q}_\alpha\cdot\mathbf{q}_\beta}\,, \tag{A8}$$

where

$$g^R_{n\beta}(|-\tfrac{1}{2}\mathbf{q}_\beta-\mathbf{q}_\alpha|)=\int_0^\infty dk\,k^2\frac{g_{n_\beta}(k)}{E-k^2-\frac{3}{4}q_\beta^2}\frac{g}{\pi k|\mathbf{q}_\alpha+\frac{1}{2}\mathbf{q}_\beta|}Q_{l_\beta}\left[\frac{k^2+|\mathbf{q}_\alpha+\frac{1}{2}\mathbf{q}_\beta|^2+R^{-2}}{2k|\mathbf{q}_\alpha+\frac{1}{2}\mathbf{q}_\beta|}\right]. \tag{A9}$$

The coupling strength of the Coulomb potential is set to $g=e^2/(2\pi^2)$. The mirroring case with the additional Coulomb interaction in the incoming subsystem can easily be found by the exchange of the initial and final states. For the graph (c) we find

$$\tilde{V}^{J\pi I_z(c)}_{N_\beta N_\alpha}(q_\beta;q_\alpha;E)=\sum_{\substack{l_\beta l_\alpha\\ aa'\mathcal{L}}}\sum_{\substack{xx'\\ dd'}}\sum_{ll'}S^{(c)}_{N_\beta N_\alpha\mathcal{L}xx'll'dd'aa'}q_\beta^{a+a'}q_\alpha^{d+d'-a-a'}B^{(c)\mathcal{L}}_{n_\beta xld,n_\alpha x'l'd'}(q_\beta,q_\alpha;E)\,. \tag{A10}$$

It should be noted here that the triangle inequalities valid for the j symbols do not lead to finite sums over x and x' for $l>0$. However the numerical convergence of these sums has already been studied in Ref. 12 and we have found again that $x_{\max}=2$ produced converged results. For N-N S-wave potentials the summation can be replaced by an analytical expression.[41]

$$\begin{aligned}B^{(c)\mathcal{L}}_{n_\beta xld,n_\alpha x'l'd'}(q_\beta,q_\alpha;E)=&\tfrac{1}{2}\int_{-1}^{+1}d(\hat{\mathbf{q}}_\alpha\cdot\hat{\mathbf{q}}_\beta)P_{\mathcal{L}}(\hat{\mathbf{q}}_\alpha\cdot\hat{\mathbf{q}}_\beta)\\&\times|\mathbf{q}_\alpha+\tfrac{1}{2}\mathbf{q}_\beta|^{x-d}|\tfrac{1}{2}\mathbf{q}_\alpha+\mathbf{q}_\beta|^{x'-d'}\int_0^\infty dk\,k^{l_\beta+l_\alpha-x-x'+2}v_C(k)\\&\times F^l_{n_\beta}(k,|\mathbf{q}_\alpha+\tfrac{1}{2}\mathbf{q}_\beta|;E-\tfrac{3}{4}q_\alpha^2)F^{l'}_{n_\alpha}(k,|\tfrac{1}{2}\mathbf{q}_\alpha+\mathbf{q}_\beta|;E-\tfrac{3}{4}q_\beta^2)\,,\end{aligned} \tag{A11}$$

with

$$F^l_{n_\beta}(k,q;z)=\tfrac{1}{2}\int_{-1}^{+1}dx\frac{|\mathbf{k}-\mathbf{q}|^{-l_\beta}g_{n_\beta}(|\mathbf{k}-\mathbf{q}|)}{z-(\mathbf{k}-\mathbf{q})^2}P_l(x),\quad x=\hat{\mathbf{k}}\cdot\hat{\mathbf{q}} \tag{A12}$$

and

$$\begin{aligned}S^{(c)}_{N_\beta N_\alpha\mathcal{L}xx'll'dd'aa'}=&4\pi\hat{L}_\beta\hat{L}_\alpha\hat{S}_\beta\hat{S}_\alpha\hat{j}_\beta\hat{j}_\alpha\hat{s}_\beta\hat{s}_\alpha\hat{l}_\beta\hat{l}_\alpha(\hat{\mathcal{L}}\hat{l}\hat{l}'\hat{d}\hat{d}')^2(\tfrac{1}{2})^{a-a'+d'}\\&\times\left[\frac{(2l_\beta+1)!(2l_\alpha+1)!(2d+1)!(2d'+1)!}{(2a)!(2d-2a)!(2a')!(2d'-2a')!(2x)!(2l_\beta-2x)!(2x')!(2l_\alpha-2x')!}\right]^{1/2}\\&\times\begin{Bmatrix}x&l&d\\0&0&0\end{Bmatrix}\begin{Bmatrix}x'&l'&d'\\0&0&0\end{Bmatrix}\sum_{\Lambda\Lambda'}(\hat{\Lambda}\hat{\Lambda}')^2\begin{Bmatrix}a&a'&\Lambda'\\0&0&0\end{Bmatrix}\\&\times\begin{Bmatrix}\Lambda'&\mathcal{L}&L_\beta\\0&0&0\end{Bmatrix}\begin{Bmatrix}d-a&d'-a'&\Lambda\\0&0&0\end{Bmatrix}\begin{Bmatrix}\Lambda&\mathcal{L}&L_\alpha\\0&0&0\end{Bmatrix}\\&\times\sum_f\hat{f}^2\begin{Bmatrix}S_\alpha&S_\beta&f\\L_\beta&L_\alpha&J\end{Bmatrix}\begin{Bmatrix}L_\alpha&L_\beta&f\\\Lambda'&\Lambda&\mathcal{L}\end{Bmatrix}\begin{Bmatrix}d'&d&f\\a'&a&\Lambda'\\d'-a'&d-a&\Lambda\end{Bmatrix}\\&\times\sum_z\hat{z}^2\begin{Bmatrix}l_\beta-x&l&z\\0&0&0\end{Bmatrix}\begin{Bmatrix}l_\alpha-x'&l'&z\\0&0&0\end{Bmatrix}\begin{Bmatrix}z&d&l_\beta\\x&l_\beta-x&l\end{Bmatrix}\\&\times\begin{Bmatrix}z&d'&l_\alpha\\x'&l_\alpha-x'&l'\end{Bmatrix}\sum_g\hat{g}^2\begin{Bmatrix}d&d'&f\\S_\alpha&S_\beta&g\end{Bmatrix}\sum_p\hat{p}^2\begin{Bmatrix}S_\beta&l_\beta&p\\s_\beta&\sigma_\beta&j_\beta\end{Bmatrix}\\&\times\begin{Bmatrix}S_\beta&l_\beta&p\\z&g&d\end{Bmatrix}\begin{Bmatrix}S_\alpha&l_\alpha&p\\s_\alpha&\sigma_\alpha&j_\alpha\end{Bmatrix}\begin{Bmatrix}S_\alpha&l_\alpha&p\\z&g&d'\end{Bmatrix}\begin{Bmatrix}\sigma_\beta&s_\beta&p\\\sigma_\alpha&s_\alpha&\sigma_\gamma\end{Bmatrix}(-1)^R\\R=&J+S_\alpha+S_\beta-L_\alpha-L_\beta+\mathcal{L}+s_\alpha-l_\beta-g+1\,.\end{aligned} \tag{A13}$$

The graph (d) is given by

$$\tilde{V}^{J\pi I_z (d)}_{N_\beta N_\alpha}(q_\beta,q_\alpha;E)=\sum_{\substack{l_\beta l_\alpha \\ \mathcal{L}l}}\sum_{acf} S^{(d)}_{N_\alpha N'_\alpha \mathcal{L} lacf} q_\alpha^{c+f} q'^{a+l-c-f}_\alpha B^{(d)\mathcal{L}}_{n_\alpha n'_\alpha la}(q_\alpha,q'_\alpha;E)\ , \tag{A14}$$

with

$$\begin{aligned} S^{(d)}_{N_\alpha N'_\alpha \mathcal{L} lacf} &= 4\pi \hat{L}_\alpha \hat{L}'_\alpha \hat{S}_\alpha \hat{S}'_\alpha \hat{j}_\alpha \hat{j}'_\alpha \hat{l}_\alpha \hat{l}'_\alpha \hat{a}(\hat{\mathcal{L}}\hat{l})^2 (\tfrac{1}{2})^a \\ &\times \left[\frac{(2l_\alpha+1)!(2l+1)!}{(2l_\alpha-2a)!(2c)!(2a-2c)!(2f)!(2l-2f)!}\right]^{1/2} \begin{pmatrix} l_\alpha-a & l & l'_\alpha \\ 0 & 0 & 0 \end{pmatrix} \\ &\times \sum_{\Lambda\Lambda'} (\Lambda\Lambda')^2 \begin{pmatrix} c & f & \Lambda \\ 0 & 0 & 0 \end{pmatrix} \begin{pmatrix} \Lambda & \mathcal{L} & L_\alpha \\ 0 & 0 & 0 \end{pmatrix} \begin{pmatrix} a-c & l-f & \Lambda' \\ 0 & 0 & 0 \end{pmatrix} \\ &\times \begin{pmatrix} \Lambda' & f & L'_\alpha \\ 0 & 0 & 0 \end{pmatrix} \sum_h \hat{h}^2 \begin{Bmatrix} l_\alpha & l'_\alpha & h \\ l & a & l_\alpha-a \end{Bmatrix} \begin{Bmatrix} L_\alpha & L'_\alpha & h \\ \Lambda' & \Lambda & \mathcal{L} \end{Bmatrix} \\ &\times \begin{Bmatrix} S_\alpha & S'_\alpha & h \\ L'_\alpha & L_\alpha & J \end{Bmatrix} \begin{Bmatrix} a & l & h \\ c & f & \Lambda \\ a-c & l-f & \Lambda' \end{Bmatrix} \sum_p \hat{p}^2 \begin{Bmatrix} l'_\alpha & l_\alpha & h \\ S_\alpha & S'_\alpha & p \end{Bmatrix} \begin{Bmatrix} s_\alpha & \sigma_\alpha & p \\ S_\alpha & l_\alpha & j_\alpha \end{Bmatrix} \begin{Bmatrix} s_\alpha & j_\alpha & p \\ S'_\alpha & l'_\alpha & j'_\alpha \end{Bmatrix} (-1)^R\ , \end{aligned}$$

$$R=J+L_\alpha+\mathcal{L}+p-a-1\ , \tag{A15}$$

and

$$\begin{aligned} B^{(d)\mathcal{L}}_{n_\alpha n'_\alpha la}(q_\alpha,q'_\alpha;E) &= (-1)^{\mathcal{L}} \tfrac{1}{2} \int_{-1}^{+1} d(\hat{q}_\alpha\cdot\hat{q}'_\alpha) P_{\mathcal{L}}(\hat{q}_\alpha\cdot\hat{q}'_\alpha) |\mathbf{q}_\alpha-\mathbf{q}'_\alpha|^{-l} v_C(|\mathbf{q}_\alpha-\mathbf{q}'_\alpha|) \\ &\times \int_0^\infty dk\, k^{l_\alpha-a+2} \frac{g^*_{n_\alpha}(k)}{E-\frac{3}{4}q_\alpha^2-k^2} F^l_{n_\alpha}\left[k,\frac{-|\mathbf{q}_\alpha-\mathbf{q}'_\alpha|}{2};E-\tfrac{3}{4}q_\alpha^2\right]\ . \end{aligned} \tag{A16}$$

Finally, we find for the isospin representation of the effective propagator,

$$G^{J\pi I_z}_{0;\nu_\gamma N_{\gamma'}}(E)=\sum_{i_{\alpha_z}} \hat{I}'_\alpha \hat{I}_\alpha \begin{pmatrix} \frac{1}{2} & i_\alpha & I'_\alpha \\ I_z-i_{\alpha_z} & i_{\alpha_z} & -I_z \end{pmatrix} \begin{pmatrix} \frac{1}{2} & i_\alpha & I_\alpha \\ I_z-i_{\alpha_z} & i_{\alpha_z} & -I_z \end{pmatrix} \tau_{\gamma;i_{\alpha_z}}(E)\ . \tag{A17}$$

[1] E. O. Alt, W. Sandhas, H. Zankel, and H. Ziegelmann, Phys. Rev. Lett. **37**, 1537 (1976).
[2] E. O. Alt, W. Sandhas, and H. Ziegelmann, Phys. Rev. C **17**, 1981 (1978).
[3] A. A. Kvitsinskii, Pis'ma Zh. Eksp. Teor. Fiz. **36**, 375 (1982) [JETP Lett. **36**, 455 (1982)].
[4] Y. A. Kuperin, S. P. Merkuriev, and A. A. Kvitsinskii, Yad. Fiz. **37**, 1440 (1983) [Sov. J. Nucl. Phys. **37**, 857 (1983)].
[5] J. L. Friar, B. F. Gibson, and C. L. Payne, Phys. Rev. C **28**, 983 (1983).
[6] J. L. Friar, B. F. Gibson, G. L. Payne, and C. R. Chen, Phys. Rev. C **30**, 1121 (1984).
[7] C. R. Chen, G. L. Payne, J. L. Friar, and B. F. Gibson, Phys. Rev. C **33**, 401 (1986).
[8] G. H. Berthold and H. Zankel, Phys. Rev. C **34**, 1203 (1986).
[9] Gy. Bencze, C. Chandler, J. L. Friar, A. G. Gibson, and G. L. Payne, Phys. Rev. C **35**, 1188 (1987).
[10] C. R. Chen, G. L. Payne, J. L. Friar, and B. F. Gibson, Phys. Rev. C **39**, 1261 (1989).
[11] G. H. Berthold, A. Stadler, and H. Zankel, Few-Body Syst., Suppl. **1**, 182 (1986).
[12] G. H. Berthold, A. Stadler, and H. Zankel, Phys. Rev. C **38**, 444 (1988).
[13] A. Stadler, Ph. D. thesis, Universität Graz, 1989.
[14] L. P. Kok and H. van Haeringen, Phys. Rev. C **21**, 512 (1980).
[15] P. Doleshall, Nucl. Phys. **A220**, 491 (1974).
[16] S. C. Pieper, Nucl. Phys. **A193**, 529 (1972); Phys. Rev. C **6**, 1157 (1972).
[17] J. Haidenbauer and W. Plessas, Phys. Rev. C **30**, 1822 (1984).
[18] H. Zankel, W. Plessas, and J. Haidenbauer, Phys. Rev. C **28**, 538 (1983).
[19] G. H. Berthold, H. Zankel, L. Mathelitsch, and H. Carcilazo, Nuovo Cimento **93A**, 89 (1986).
[20] J. Haidenbauer, private communication.
[21] L. Crepinsek, C. B. Lang, H. Oberhummer, W. Plessas, and H. F. K. Zingl, Acta. Phys. Austriaca **42**, 139 (1975).
[22] M. Lacombe, B. Loiseau, J. M. Richard, R. Vinh Mau, J. Côté, P. Pires, and R. de Tourreil, Phys. Rev. C **21**, 861 (1980).
[23] F. Calogero, Nuovo Cimento **27**, 267 (1963).
[24] A. R. Edmonds, *Angular Momentum in Quantum Mechanics*, Revised ed. (Princeton University Press, Princeton, 1968).

[25]*Proceedings of the 3rd International Symposium on Polarization Phenomena in Nuclear Reactions,* edited by H. H. Barschall and W. Haeberli (University of Wisconsin Press, Madison, 1971).
[26]D. C. Kocher and T. B. Clegg, Nucl. Phys. **A132**, 455 (1969).
[27]W. Trächslin and L. Brown, Nucl. Phys. **A90**, 593 (1967); W. Trächslin, L. Brown, T. B. Clegg, and R. G. Seyler, Phys. Lett. **25B**, 585 (1967).
[28]R. E. White, W. Grüebler, V. Köneg, R. Rislerr, A. Ruth, P. A. Schmelzbach, and P. Marimier, Nucl. Phys. **A180**, 593 (1972).
[29]R. Sherr, J. M. Blair, H. R. Kratz, C. L. Bailey, and R. F. Taschek, Phys. Rev. **72**, 662 (1947).
[30]R. E. White, W. Grüebler, B. Jenny, V. König, P. A. Schmelzbach, and H. R. Bürgi, Nucl. Phys. **A321**, 1 (1979).
[31]P. Doleschall, W. Grübler, V. König, P. A. Schmelzbach, F. Sperisen, and B. Jenny, Nucl. Phys. **A380**, 72 (1982).
[32]W. Tornow, J. Herdtweck, W. Arnold, and G. Mertens, Phys. Lett. B **203**, 341 (1988).
[33]P. A. Schmelzbach, W. Grüebler, R. E. White, V. König, R. Risler, and J. Marmier, Nucl. Phys. **A197**, 273 (1972).
[34]R. G. Seyler, Nucl. Phys. **A124**, 253 (1969).
[35]W. Grüebler, Nucl. Phys. **A353**, 31c (1981).
[36]G. H. Lamot, C. Fayard, C. Elbaz, Lett. Nuovo Cimento **9**, 653 (1974).
[37]E. O. Alt, W. Sandhas, and H. Ziegelmann, Nucl. Phys. **A445**, 429 (1985).
[38]In an energy-dependent phase shift analysis comparing data between $E_{\text{lab}}^{p}=0.4$ and 3.0 MeV by Huttel *et al.*, Nucl. Phys. **A406**, 443 (1983), significantly bigger doublet P waves were found although also with a rather strong splitting.
[39]H. Zankel and G. M. Hale, Phys. Rev. C **24**, 1384 (1981).
[40]H. Witala, W. Glöckle, and T. Cornelius, Nucl. Phys. **A491**, 157 (1989).
[41]H. Zankel and H. Zingl, Acta. Phys. Austriaca **44**, 245 (1976).
[42]K. L. Kowalski, Phys. Rev. Lett. **15**, 798 (1965).
[43]H. P. Noyes, Phys. Rev. Lett. **15**, 538 (1965).